Mottl, M.J., Davis, E.E., Fisher, A.T., and Slack, J.F. (Eds.), 1994
Proceedings of the Ocean Drilling Program, Scientific Results, Vol. 139

21. FLUID INCLUSION PETROGRAPHY AND MICROTHERMOMETRY OF THE MIDDLE VALLEY HYDROTHERMAL SYSTEM, NORTHERN JUAN DE FUCA RIDGE[1]

Jan M. Peter,[2] Wayne D. Goodfellow,[2] and Matthew I. Leybourne[2]

ABSTRACT

Middle Valley is a hydrothermally active, sediment-covered rift at the northernmost end of the Juan de Fuca Ridge. Two hydrothermal centers are known from previous work: (1) a 60-m-high sediment mound with a 35-m-high inactive sulfide mound and two 20-m-high sulfide mounds 330 m to the south, one of which is known to be active, and (2) several mounds with attendant active hydrothermal chimneys. These sites (Sites 856 and 858, respectively), as well as other adjacent areas (Sites 857 and 855), were drilled during Leg 139 of the Ocean Drilling Program. Fluid inclusion petrographic observations and microthermometric measurements were made on a variety of samples and minerals recovered from these cores: (1) quartz from hydrothermally altered sediment; (2) low iron sphalerite and interstitial dolomite in massive sulfide; (3) calcite-sulfide veins cross-cutting sediment; (4) calcite and anhydrite concretions in sediment; (5) anhydrite veins cross-cutting sediment; and (6) wairakite and quartz veins cross-cutting mafic sills and sediment. Trapping temperatures of fluid inclusions in hydrothermal alteration minerals precipitated with massive sulfides range between 90° and 338°C. Fluid inclusions in calcite in carbonate concretions indicate these concretions formed between 112° and 192°C. Anhydrite in veins and concretions was precipitated between 137° and 311°C. Quartz-wairakite-epidote veins in mafic sills and hydrothermally altered sediment were precipitated between 210° and 350°C. For all inclusions, there is a general increase in minimum trapping temperatures with increasing subsurface depth for all sites, with temperatures ranging from around 100°C at 2400 meters below sea level to around 275°C at 3100 mbsl. Eutectic and hydrohalite melting temperatures indicate that Ca, Na, and Cl are the dominant ionic species present in the inclusion fluids. Salinities for most inclusion fluids range between 2.5 and 7.0 equivalent weight percent NaCl. Most analyses are between 3 and 4.5 eq. wt% NaCl and similar to ambient bottom water, pore fluids, and vent fluid from Site 858. Trapped fluids are modified seawater, and there is no evidence for a significant magmatic fluid component. Oxygen isotopic compositions for fluids from which calcite concretions were precipitated, calculated from isotopic analyses of carbonates formed at low temperatures (133° to 158°C from fluid inclusions), are significantly enriched in ^{18}O ($\delta^{18}O$ = +9.3‰ to +13.2‰), likely due to reaction with subsurface sediments at low water/rock ratios. Calcite that formed at higher temperatures (233°C) in hydrothermally altered sediment was precipitated from fluid only slightly enriched in ^{18}O ($\delta^{18}O$ = +0.4‰). Estimated carbon isotope compositions of the fluid vary between $\delta^{13}C$ = –7.0‰ and –35.4‰ and are similar to the measured range for vent fluids.

INTRODUCTION

Middle Valley (MV) is a sedimented rift on the east flank of Endeavor Segment of the Juan de Fuca Ridge, situated 300 km west of the continental margin of British Columbia and Washington (Fig. 1) (Davis et al., 1987). At least 350 m of turbiditic sediments overlie the basaltic basement (Davis, Mottl, Fisher, et al., 1992). Drill cores were recovered during Leg 139 of the Ocean Drilling Program (ODP) from the two areas of known hydrothermal venting and sulfide precipitation: (1) active hydrothermal vents termed the area of active venting (AAV), and (2) an older, hydrothermally inactive massive sulfide mound, referred to as Bent Hill (BH). At these sites, hydrothermal precipitates form mounds and chimneys at around 2450 m water depth.

Here we present fluid inclusion petrography and microthermometry results obtained from samples recovered from the MV hydrothermal system during Leg 139. Previous physical and chemical measurements of actively venting hydrothermal fluids (Butterfield et al., this volume; Franklin and Leg 139 Scientific Party, 1992; Lydon et al., 1992) and downhole temperature profiles obtained during Leg 139 provide information on current hydrothermal conditions. Fluid inclusions, however, allow the determination of paleo-hydrothermal conditions. Samples studied include: (1) quartz from indurated sediments that are interpreted to represent a high-temperature quartz-muscovite-chlorite upflow zone (BH); (2) quartz-wairakite-epidote veins from the hydrothermal reaction zone (Site 857) and upflow zone (AAV); (3) carbonate and anhydrite from the outer lower temperature margin of the upflow zone at AAV; and (4) carbonate and sphalerite from massive sulfide at BH.

Previous work on two-phase, aqueous inclusions in anhydrite from active chimneys at AAV reported temperatures of 265°C, comparable to measured vent temperatures up to 276°C, and salinities between 2.2 and 4.0 equivalent weight percent NaCl (calculated from the freezing data of Leitch, 1991). Barite from a hydrocarbon-bearing, clay-rich, inactive chimney contains primary aqueous inclusions with homogenization temperatures of 170°C and hydrocarbon-bearing inclusions with homogenization temperatures of 110°C (Leitch, 1991). Simoneit et al. (1992) have estimated that hydrothermal petroleum within chimneys was formed at temperatures below about 120°C from 29-ka carbon. No hydrocarbon-bearing inclusions were observed in the present study.

GEOLOGICAL SETTING

Site 856 (Bent Hill)

BH is a 500-m-diameter by 60-m-high, subcircular uplifted block of sediment in the eastern part of MV (Fig. 1) (Davis and Sawyer, 1987; Goodfellow and Blaise, 1988; Franklin et al., 1991; Goodfellow and Franklin, in press). Sulfides are exposed in a 35-m-high by 200-m-wide sulfide mound about 100 m south of BH (Fig. 2). A single mound 330 m south of BH with a 264°C vent was discovered during dives with the submersible *ALVIN* (Franklin et al., 1991) (Fig. 2). Drilling during Leg 139 recovered 96 m of massive sulfide from Hole 856H and 65 m from Hole 856G. In this study, samples from four holes drilled at Site 856 were investigated. Hole 856B, on the southern margin of BH (Fig. 2), intersected slumped massive sulfide and variably altered hemipelagic and turbiditic sediment. The bottom of this hole (Core 139-856B-15X) consists of indurated siltstone to sandstone that has been altered to an assemblage of quartz–Fe-rich chlorite–muscovite–rutile

[1] Mottl, M.J., Davis, E.E., Fisher, A.T., and Slack, J.F. (Eds.), 1994. *Proc. ODP, Sci. Results*, 139: College Station, TX (Ocean Drilling Program).

[2] Mineral Resources Division, Geological Survey of Canada, 601 Booth Street, Ottawa, Ontario K1A 0E8, Canada.

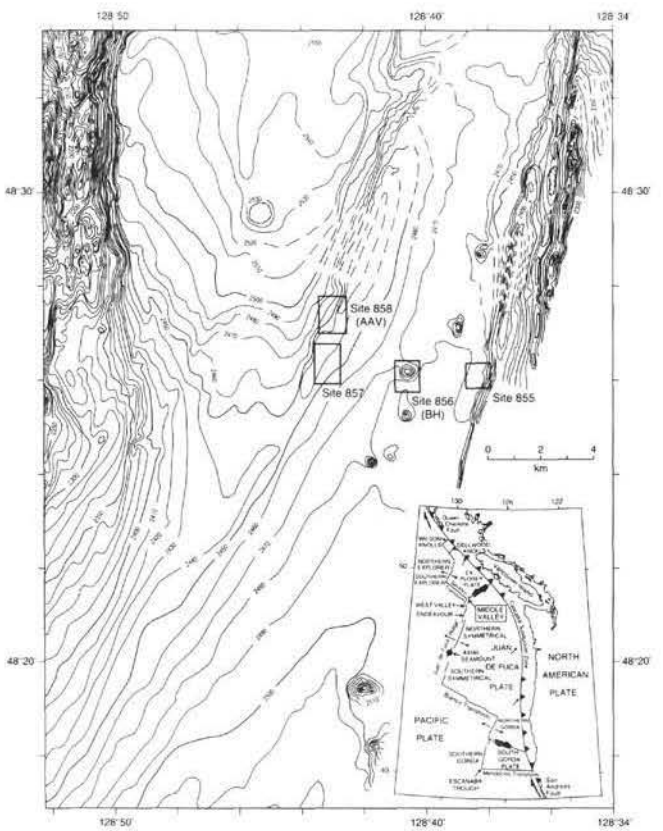

Figure 1. Location map of Middle Valley hydrothermal sites (AAV = area of active venting; BH = Bent Hill). Inset shows location of Middle Valley on the Juan de Fuca Ridge System.

± chalcopyrite ± pyrite ± pyrrhotite. Hydrothermal alteration consists of up to 2 mm aggregates of chalcopyrite, pyrite, and quartz which entirely replace detrital minerals (Table 1; Goodfellow and Peter, this volume). Hole 856F, just south of BH (Fig. 2), contains sulfide (pyrite, pyrrhotite, chalcopyrite, and sphalerite) clasts within a finer grained sediment matrix. Cores from Holes 856G and 856H (Fig. 2) from the most northerly sulfide mound consist predominantly of massive sulfide (pyrite-pyrrhotite-sphalerite-chalcopyrite-magnetite) with interstitial Mg-silicates (talc, serpentine, Mg-rich chlorite) and carbonate, and cross-cutting carbonate and silicate veins. This carbonate is principally dolomite, with lesser calcite, magnesite, and siderite (Leybourne and Goodfellow, this volume). Two generations of sphalerite occur in Hole 856G: early, opaque, high-iron and later, translucent, low-iron sphalerite. Due to the opacity of the former variety, only inclusions in low-iron sphalerite could be studied. In summary, Site 856 represents a fossil, inactive, high-temperature upflow zone.

Site 857

Site 857 (Fig. 1) is located 5.2 km west of the normal fault scarp that forms the eastern topographic boundary of MV, and is about 1.5 km east of the sediment-buried fault that forms the current structural boundary of the central part of the rift. Sediments here consist of late Pleistocene to Holocene interbedded hemipelagic mud and turbiditic silt and sand that have been intruded by mafic sills below 465 meters below seafloor (mbsf). Site 857 is an area of high heat flow, typically over 0.8 W m^{-2} (Davis, Goodfellow, et al., 1987), and is 1.6 km south of AAV (Site 858), where fluids actively vent at temperatures up to 276°C (Franklin et al., 1991). The three holes drilled at this site continuously sample the stratigraphic sequence to 936 mbsf. Samples from Holes 857C and 857D were used in this study. The lower portions of

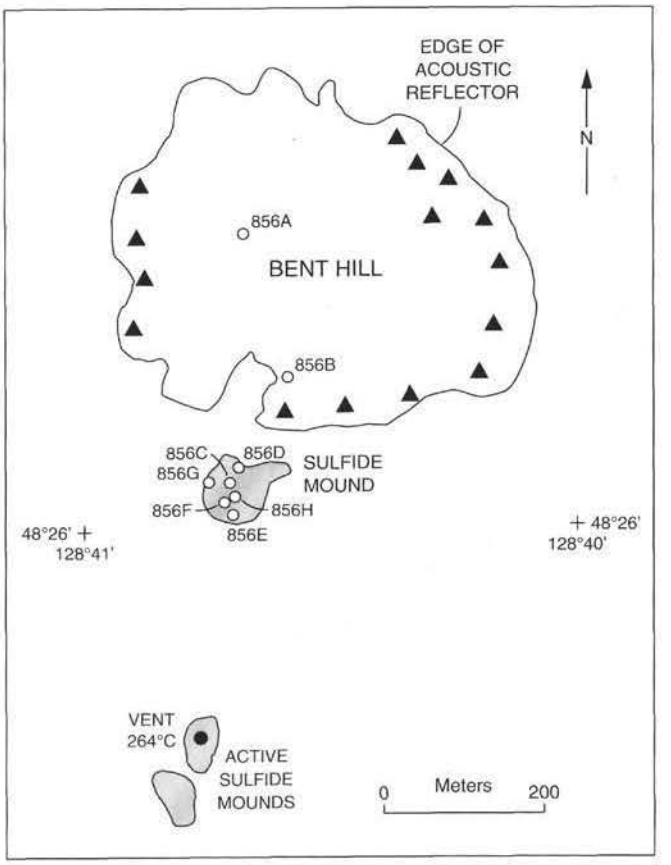

Figure 2. Map showing the BH sediment mound mapped by the limit of the acoustically reflective area, the inactive BH sulfide deposit near the southern flank of the sediment mound, and two sulfide mounds about 330 m south of BH, one of which is actively venting high-temperature fluids from an anhydrite-sulfide chimney. Also shown are locations of ODP drill holes, sulfide outcrop, and talus.

Holes 857C and 857D are composed of indurated, hydrothermally altered siltstone to claystone, with cross-cutting hydrothermal veins of quartz, wairakite, epidote, and pyrite. Mafic sills are common here (Stakes and Franklin, this volume) and host two styles of cross-cutting veins: (1) iron sulfide–chlorite ± epidote veins, and (2) quartz–wairakite–epidote ± actinolite veins (Davis, Mottl, Fisher, et al., 1992). In summary, Site 857 is a reaction zone for fluids that are presently venting at Site 858 (Goodfellow and Peter, this volume).

Site 858 (Area of Active Venting)

This site hosts a flat, north-trending, 700-m by 400-m hydrothermally active area referred to as AAV (Goodfellow and Blaise, 1988) (Fig. 1). Dives with the submersible *ALVIN* during the summer of 1990 recorded temperatures of hydrothermal fluid venting up to 276°C from chimneys on mounds typically measuring 25 m in diameter and 7 m in height (Franklin et al., 1991). Hole 858A, drilled 100 m west of AAV and Hole 858C, 70 m west of the vent field (Fig. 3), cored moderately altered hemipelagic and turbiditic sediments that host 1- to 8-cm-diameter carbonate concretions, and anhydrite nodules and veins. Carbonate also infills and replaces worm burrows at AAV (Goodfellow et

al., 1994). Hole 858B was drilled a few meters from a 276°C vent, and Mg-rich sediments and massive sulfide with interstitial carbonate were recovered. Hole 858F was drilled near the center of the vent field (Fig. 3). Cores are altered and indurated sandstone to claystone with rare matrix wairakite, and have been cut by quartz-wairakite-epidote veins. In summary, Site 858 is a presently active, low-temperature hydrothermal system which is not precipitating significant sulfide mineralization; hydrothermal mineralization is predominantly anhydrite chimneys on sediment mounds (Goodfellow and Franklin, in press).

ANALYTICAL METHODS

Fluid inclusion microthermometric measurements were made on crystals that were hand-picked from friable and readily disaggregated samples, and on doubly polished thin sections made from indurated and/or fine-grained samples, prepared by the method of Holland et al. (1978). Homogenization temperatures and freezing point depressions were determined with a Linkam TH600 fluid inclusion stage (Shepherd, 1981) calibrated according to the method of MacDonald and Spooner (1981). Calibrations were made using pure substances and Merck® chemical standards of known melting temperatures. The accuracy of a temperature measurement is estimated to be within ±7°C at around 400°C and ±0.2°C at and below 0°C, and the reproducibility is estimated at ±2°C around 300° to 400°C and ±0.2°C at and below 0°C. For freezing measurements, fluid inclusions were supercooled to −100°C or cooler until completely frozen and were then slowly heated.

Four samples of calcite and two samples of dolomite for which fluid inclusion trapping temperatures (T_t) were determined were selected for stable carbon and oxygen isotope analysis. Samples were powdered and CO_2 was extracted with 100% H_3PO_4 according to the method of McCrea (1950) as follows: samples were reacted for 2 hr at 25°C to extract calcite CO_2. After calcite was extracted, samples were reacted for an additional 12 hr, and this CO_2 was disposed; the remaining sample was then reacted for 12 to 24 hr at 50°C to extract dolomite CO_2. Carbonate minerals were mechanically separated at the Geological Survey of Canada and chemically purified and analyzed at the Ottawa-Carleton Geoscience Centre (OCGC) Stable Isotope facility at the University of Ottawa. Isotope ratios were measured on a VG Micromass 602 mass spectrometer. The oxygen isotope data are reported relative to standard mean ocean water (SMOW), and the carbon isotope compositions to the Peedee belemnite (PDB) reference standard. Precision for both the $\delta^{18}O$ and $\delta^{13}C$ analyses is ±0.1‰ (2σ).

RESULTS

Mineralogy and Fluid Inclusion Petrography

Fluid inclusions were measured in quartz, calcite, dolomite, and anhydrite, which are present as alteration minerals in the groundmass of hydrothermally altered sediment; in sphalerite and dolomite in massive sulfide; in calcite in carbonate concretions; and in quartz, wairakite, and anhydrite in veins. Summary descriptions of the samples studied, their mineralogy, and fluid inclusion petrography are given in Table 1. Additionally, Leybourne and Goodfellow (this volume) give a more detailed description of the style and mode of alteration minerals within which we measured fluid inclusions. Plate 1 is a composite of transmitted light photomicrographs of fluid inclusion sections of representative samples. Samples include sulfide with interstitial carbonate without cross-cutting veinlets (Pl. 1A) and with cross-cutting veinlets (Pl. 1B), hydrothermally altered (quartz and sulfides), fine-grained laminated sediment without cross-cutting veinlets (Pl. 1C) and with cross-cutting veinlets (Pl. 1D), mafic sill with cross-cutting quartz-wairakite-epidote veinlets (Pl. 1E), and coarse-grained carbonate concretions (Pl. 1F). Authigenic quartz from hydrothermally altered sediment may be anhedral to euhedral and replaces detrital quartz, feldspar, and other constituents (Leybourne and Goodfellow, this volume). Calcite and dolomite within hydrothermally altered sediment is generally anhedral, whereas that from cross-cutting veinlets generally is subhedral to anhedral.

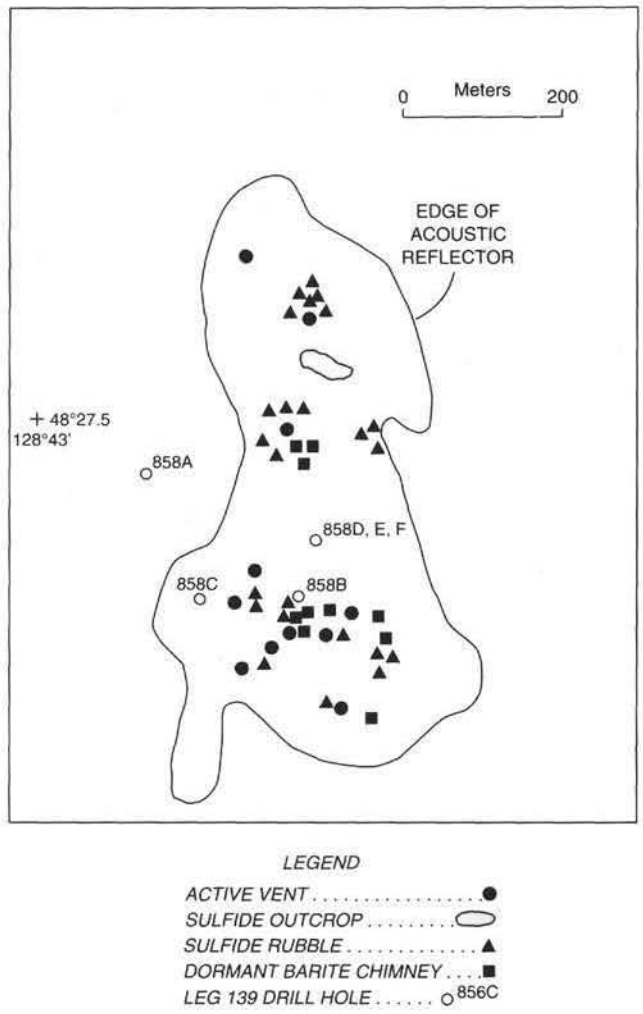

Figure 3. Map of the AAV showing the limit of the acoustically reflective area and locations of ODP drill holes, active vents, sulfide outcrop, sulfide rubble, and barite chimneys.

Fluid inclusions have been classified according to the criteria of Roedder (1984) to discriminate between primary and secondary inclusions, and descriptions of these inclusion types are given below. Both primary inclusions, which are interpreted to contain the extant hydrothermal fluid during mineral growth, and secondary inclusions, which are interpreted to have trapped fluids after mineral precipitation, such as along healed fractures (Roedder, 1984), are present in all sample types. As pointed out by Peter and Scott (1988) and Vanko (1988), however, given the rapid precipitation of hydrothermal minerals in such seafloor settings, fluids in primary inclusions may actually be introduced along fractures in the host minerals and be preserved in secondary-appearing inclusions. Thus, inclusions classified as secondary here may actually be pseudosecondary inclusions according to the criteria of Roedder (1984).

Primary Inclusions

Primary inclusions occur as either isolated inclusions, as small, three-dimensional clusters of inclusions located randomly within individual crystals, and as inclusions that occur with minute solid inclusions along growth zones in carbonate. Primary inclusions occur in

Table 1. Description of Middle Valley fluid inclusion samples used in this study.

Sample Number	Description	Mineralogy	Fluid Inclusion Petrography & Comments
139-856B-15X-2, 67-69 cm	Medium light grey, laminated, indurated, silty sandstone mineralized with patches (to 2 mm) of Cp and Py accompanied by Qz.	Auth. Cly (40%-50%), auth. Qz (40%), auth. Ch (5%), Ru(<1%), Py (1%), Cp (1%).	Some Py as up to 0.8 mm euhedra. Fluid inclusions measured in auth. Qz which occurs as disseminated, <0.25 mm diameter, anhedral, unzoned crystals which replace detrital Qz. Moderately abundant fluid inclusions homogeneously distributed throughout crystals. Primary inclusions are isolated and have hexagonal negative crystal and rectangular cross-sections.
139-856F-2X-CC, 23-25 cm	Lithified sand with sulfide clasts within Carb matrix.	Carb (40%), Py (25%), Fe Ox (15-20%), Po (5%), Sp (8%-10%), Mt (2-3%), Cp (<1%).	Fluid inclusions measured in Do which occurs as <0.5 mm, cloudy to clear, euhedral to subhedral crystals interstitial to sulfides. Moderately abundant fluid inclusions homogeneously distributed throughout crystals. Primary inclusions have rectangular morphologies.
139-856G-7R-4, 4-6 cm	Dense to loose network of interlocking Py, with inclusions of Cp and early, high-Fe Sp, and interstitial and rimming low-Fe Sp.	Py (75-80%), Sp (20%-25%), Cp (<1%).	Fluid inclusions measured in low-iron Sp which occurs as <0.5 mm anhedral rims on high-Fe Sp. Moderately abundant fluid inclusions homogeneously distributed throughout crystals. Primary inclusions have hexagonal negative crystal , rounded and oval morphologies.
139-856H-3R-2, 16-18 cm	Heterogeneous medium to c.gr. Py and Mt, with interstitial Carb and Cly matrix.	Py (40%), Do (18%), auth. Cly & Ch (12%), Mt (10%), Po (3%), Sp (3%), Cp (3%), Ht and Gt (<1%).	Fluid inclusions measured in Do which is interstitial to Sulf. and occurs as subhedral, 0.02 to 0.3 mm, zoned crystals with common Mt inclusions and abundant fluid inclusions. Few irregularly-shaped fluid inclusions homogeneously distributed throughout crystals.
139-856H-3R-2, 84-87 cm	Heterogeneous medium to c.gr. Py + Mt, with interstitial Do. Sample has a large subrounded clast of Py-Po.	Do(50%), Py (25%), Po (10%), Sp (10%), Mt (3%), auth. Cly (1%), Cp (<1%).	Fluid inclusions measured in interstitial Do which occurs as anhedral to subhedral, 0.02 to 0.5 mm, partly zoned crystals. Few irregularly-shaped fluid inclusions homogeneously distributed throughout crystals and not restricted to certain zones.
139-857C-60R-2, 28-30 cm	Mafic sill with 0.2 to 1-mm-wide crosscutting Qz-Wa-Ep vein.	Plag, Cpx, Ox, Ch, Sulf, Ep, Qz, Wa.	Moderately abundant randomly distributed primary fluid inclusions with rounded, oval, and negative crystal morphologies and clusters of moderately abundant irregular secondary inclusions along healed microfractures. Primary inclusions measured in vein Qz which occur as 0.2 to 0.5 mm, anhedral to crystals intergrown with fibrous epidote.
139-857C-61R-2, 4-6 cm	Mafic sill with 2 to 10-mm-wide crosscutting Qz-Wa-Ep vein.	Plag, Cpx, Ox, Ch, Sulf, Ep, Qz, Wa.	Moderately abundant randomly distributed primary fluid inclusions with rounded, oval, and negative crystal morphologies and clusters of moderately abundant irregular secondary inclusions along healed microfractures. Primary inclusions measured in vein Qz which occur as 0.2 to 3 mm, anhedral to euhedral (hexagonal) crystals intergrown with epidote.
139-857C-62R-1, 67-69 cm	Mafic sill with 20 to 30-mm-wide crosscutting Qz-Wa-Ep vein.	Plag, Cpx, Ox, Ch, Sulf, Ep, Qz, Wa.	Abundant randomly distributed primary fluid inclusions with rounded, oval, and negative crystal morphologies and clusters of minor irregular secondary inclusions along healed microfractures. Primary inclusions measured in vein Qz which occur as 0.2 to 5 mm, anhedral to euhedral interlocking crystals intergrown with fibrous epidote.
139-857C-64R-2, 74-76 cm	2 to 3-mm-wide Qz-Wa-Ep vein crosscutting mafic sill.	Plag, Cpx, Ox, Ch, Sulf., Ep, Qz, Wa.	Fluid inclusions measured in vein Wa which occurs as <0.1 to 0.2 mm diameter, subhedral crystals intergrown with Qz and Ep. Abundant irregularly shaped fluid inclusions distributed throughout crystals in discrete patches. Inclusions have rounded, oval, to irregular morphologies.
139-857D-1R-1, 137-139	Medium light gray indurated siltstone with a 0.2-mm-wide, crosscutting Qz-Ep vein.	Qz(50%-60%), Cly/Ch (15%-20%), Fs (10%-15%), Ep (1%), Mi (1%), Py (tr).	Fluid inclusions measured in vein Qz which occurs as 0.01 to 0.1 mm, anhedral, clear, unzoned crystals. Few fluid inclusions distributed throughout crystals. Inclusions have rounded, oval, to rectangular morphologies.
139-857D-11R-1, 1-3 cm	Light gray, indurated sandstone with 5-mm-wide crosscutting vuggy Qz-Wa-Ep vein with euhedral Qz crystals.	Qz, Fs, Ch, Ep, & Wa + Qz vein fill.	Fluid inclusions measured in hand-picked vein Qz which occurs as euhedral, hexagonal, 1-3 mm long crystals with rare to common fluid inclusions. Few isolated primary inclusions with rectangular morphologies and abundant secondary inclusions with irregular to needle-like morphologies along healed fracture planes.

Table 1 (continued).

SAMPLE	DESCRIPTION	MINERALOGY	FLUID INCLUSION PETROGRAPHY & COMMENTS
139-857D-12R-1, 88-90 cm	Mafic sill with 0.3 to 1-mm-wide crosscutting, anastomosing Qz-Wa-Ep vein.	Plag, Cpx, Ox, Ch, Sulf, Ep, Qz, Wa.	Abundant primary fluid inclusions with rounded, oval, and irregular morphologies. Abundant secondary fluid inclusions along healed microfractures. Secondary inclusions are oval to elongate, and some have highly irregular morphologies. Some adjacent secondary inclusions have varying phase ratios. Primary inclusions measured in vein Qz and Wa which occur as 0.01 to 0.1 mm, anhedral interlocking crystals.
139-858A-28X-CC, 4-5 cm	Medium gray, indurated, thinly laminated siltstone with rounded clusters of radiating Carb crystals and crosscutting 0.01 to 1.5-mm-wide tension gash(?) veins filled with An.	An (100% in vein), Cly (45%), Qz (30%), Ch (13%), Carb (5%), Fs (3%-5%), Mi (2%), Py (tr).	Fluid inclusions measured in vein An which occurs as 0.2 to 3 mm long, tabular, euhedral crystals. Few to moderately abundant primary inclusions occur as rounded and elongate morphologies, with latter inclusions restricted to cleavages.
139-858A-29X-1, 30-32 cm	Light gray, indurated sandstone with crosscutting, 3-5 mm wide An vein.	An (100% in vein), Qz (45%), auth. Cly (40%), Fs (5-10%), Carb (2%-3%), Ch (1%), Py (1%).	Fluid inclusions measured in vein An which occurs as <0.2 mm euhedral to subhedral crystals. Few to moderately abundant, rounded to oval inclusions distributed throughout crystals in discrete patches.
139-858B-2H-3, 113-115 cm	Brecciated turbiditic sand with minor Cly; contains disseminated Py and large, auth. An crystals.	No thin section. An, Cly, Py.	Fluid inclusions measured in hand picked, 0.2 to 3 mm diameter, subhedral to euhedral An crystals. Minor isolated primary inclusions with rectangular and rectilinear, stepped morphologies controlled by cleavages. Minor secondary inclusions with irregular morphologies occurring along healed fracture planes.
139-858B-2H-4, 43-45 cm	Olive gray-brown, non-indurated, silty Cly with common disseminated Py and An.	No thin section. Cly, Py, An.	Fluid inclusions measured in hand picked, 0.2 to 1 mm diameter, subhedral An crystals. Minor inclusions with irregular, elongate morphologies controlled by cleavages.
139-858C-3H-1, 78-81 cm	Carb concretion with intricate network of crosscutting, 0.1 to 2 mm wide veinlets of Ca-Py.	Ca (90%), Py (2%-3%), Ch (1%-2%), Qz (1%), Mi (<1%), Plag (rare).	Fluid inclusions measured in vein Ca which occurs as 0.025 to 1 mm diameter subhedral crystals. Few isolated, irregular to rounded inclusions distributed throughout crystals.
139-858C-3H-1, 145-150 cm	Ca concretion crosscut by 1 to 2-mm-wide veins of coarser-grained Ca in medium light olive-grey, indurated silty Cly.	No thin section. Ca, Cly.	Fluid inclusions measured in hand picked, 1 to 2 mm diameter vein Ca crystals. Moderately abundant irregular, rounded and elongate secondary inclusions along healed fracture planes.
139-858C-3H-2, 10-15 cm	Ca concretion in light gray-olive, indurated silty Cly.	Ca (95%), Py (3%), Qz (1%-2%), Fs (tr), Ch (tr), Sp (rare).	Pyrite is framboidal. Fluid inclusions measured in hand-picked, 0.025 mm, anhedral Ca crystals. Abundant rounded, rectangular, irregular to elongate primary and secondary inclusions distributed throughout crystals.
139-858C-3H-3, 22-24 cm	Light olive-grey, non-indurated clayey-silt with Ca crystals up to 4 mm in diameter and rare patches of Sulf.	No thin section. Ca, Qz, Fs.	Fluid inclusions measured in hand picked, 1 to 4 mm diameter, euhedral Ca crystals. Moderately abundant, large, rounded primary inclusions randomly distributed throughout crystals.
139-858F-2R-CC, 8-11 cm	Medium light gray, extremely indurated siltstone with a 3-mm-thick, crosscutting Qz-Wa vein. Adjacent to the vein is a 5 to 8-mm-wide zone containing rounded bundles of Ch crystals.	Cly & Ch (85%-90%), Qz & Fs (5%-10%), Wa (2%), Py (rare), Mi (rare).	Fluid inclusions measured in vein Wa which occurs as 1 to 2 mm diameter, subhedral crystals. Abundant rounded to oval primary inclusions distributed throughout crystals.
139-858G-16R-1, 77-79 cm	Mafic sill with 0.2 to 1.5-mm-wide crosscutting Qz-Wa-Ep vein.	Plag, Cpx, Ox, Ch, Sulf, Ep, Qz, Wa.	Fluid inclusions measured in vein Qz which occur as 0.01 to 0.1 mm, anhedral to euhedral interlocking crystals. Moderately abundant, randomly distributed inclusions with rounded, oval, and negative crystal morphologies.

Abbreviations: Ab = albite, An = anhydrite, auth. = authigenic, Ca = calcite, Carb = carbonate, c.gr. = coarse grained, Ch = chlorite, Cly = clay, Cp = chalcopyrite, Cpx = clinopyroxene, Do = dolomite, Ep = epidote, Fe = iron, Fs = feldspar, Gt = goethite, Ht = hematite, K-spar = K-feldspar, Mi = mica, Mt = magnetite, Ox = oxide, Plag = plagioclase, Po = pyrrhotite, Py = pyrite, Qz = quartz, Ru = Rutile, Sp = sphalerite, Sulf. = sulfides, tr = trace, Wa = wairakite.

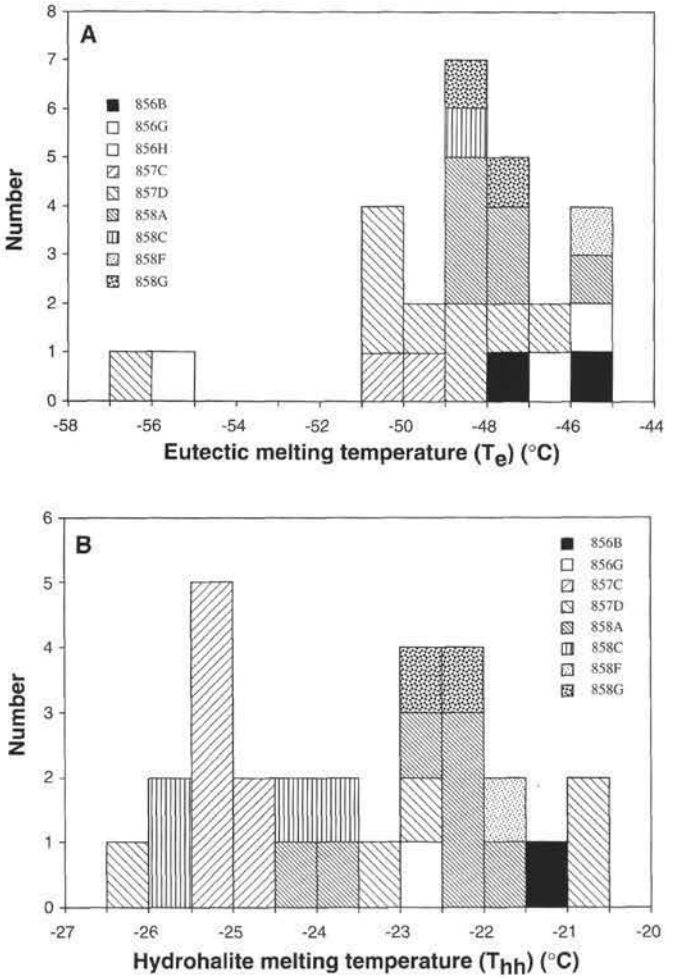

Figure 4. **A.** Frequency histogram of all observed eutectic melting temperatures for MV fluid inclusions. **B.** Frequency histogram of all observed hydrohalite melting temperatures for MV fluid inclusions.

quartz (Pl. 2A, -B, -C), sphalerite (Pl. 2D), anhydrite (Pl. 3A, -B), calcite and dolomite (Pl. 3C, -D), and wairakite (Pl. 3E). Primary inclusions in quartz range in diameter from <3 to about 15 µm, and are generally oval, circular, or hexagonal in cross section (Pl. 2A, -B, -C). Their size is generally uniform within a crystal. Primary inclusions in low-iron sphalerite range from <4 to ≈30 µm, and are oval, circular, or elongate (Pl. 2D) in cross section or display negative crystal forms. Primary inclusions in anhydrite range from 2 to 70 µm in diameter and are square, rectangular (Pl. 3A) and needle-like (Pl. 3B) in form. The orientation of these inclusions is controlled by the crystallographic axes of the anhydrite crystals. Primary inclusions in calcite vary in diameter between 2 and 180 µm and in dolomite between 2 and 27 µm, and are oval, elongate, rectangular, and irregular in cross-section (Pl. 3C, -D). Inclusions in carbonate minerals are generally randomly distributed, although some samples display conspicuous growth zoning with individual zones marked by fluid inclusions and minute solid inclusions (Pl. 3C, -D). Primary inclusions in wairakite range from <5 to about 75 µm in diameter and are generally oval, circular, and elongate in cross section (Pl. 3E).

Primary inclusions in all sample types contain two phases, an aqueous liquid and a vapor bubble, and no daughter minerals. All primary inclusions have uniform phase ratios with the vapor bubbles comprising 5 to 20 volume percent (vol%) of the inclusion (e.g., Plate 2A, -B, -C,-D, and 3A, -B, -C, -D, -E); on this basis, these inclusion fluids do not appear to have undergone boiling or phase separation at the site of mineral precipitation.

One primary fluid inclusion from Sample 139-858A-29X-1, 30–32 cm, a hydrothermally altered, fine-grained sediment with a cross-cutting veinlet of anhydrite was observed to contain three phases (CO_2 vapor bubble within a CO_2 liquid bubble in aqueous liquid). This is the only such inclusion of its type observed in all the samples examined and, due to its scarcity, we are unable to ascertain its origin and genetic relation to the MV hydrothermal systems.

Secondary Inclusions

Secondary inclusions comprise the majority of the inclusions present in many of the samples. Secondary inclusions generally contain two phases, an aqueous fluid and a vapor bubble, range from 1 to >30 µm in diameter, and are typically elongate or irregular. They occur as discontinuous planar arrays or trails along healed microfractures. Such inclusions were trapped after the brittle fracturing of the host minerals. Within a sample only one generation of secondary inclusions are present, and no cross-cutting trails of inclusions were observed. Trails of inclusions along healed microfractures were not observed to cut across grain boundaries, which suggests that fluid movement was predominantly along grain boundaries.

In certain samples, some adjacent secondary inclusions possess widely differing phase ratios. In some of these inclusions, clear evidence of necking was observed, with thin, faint hairline fractures connecting nearby inclusions. However, in other inclusions with widely different phase proportions, necking has proceeded to a greater degree, and only careful examination of both petrographic and microthermometric characteristics could be used to discern between necking and phase separation processes. Necking can result in vapor-rich inclusions, as suggested by the presence of single-phase, liquid-only inclusions (Bodnar et al., 1985). As pointed out by Bodnar et al. (1985), the presence of liquid-only inclusions in the vicinity of vapor-rich or one-phase vapor inclusions indicates that necking rather than entrapment of boiling inclusion fluids occurred. The co-occurrence of adjacent liquid-only and vapor-rich inclusions along with inclusions of widely different phase ratios in the MV samples, particularly in quartz and wairakite from quartz-wairakite-epidote veins in mafic sill samples, indicates that such inclusions are the products of post-entrapment necking.

Fluid Inclusion Microthermometry

On heating of frozen inclusions, eutectic melting (T_e) occurred between –56.4° and –45.9°C (Fig. 4A). In many of the inclusions, eutectic melting was recognized by the inclusions suddenly becoming more translucent in places. In the smaller inclusions, it was difficult to accurately observe the onset of melting due to the small amount of melt formed at the eutectic; as a result, many of the measured values may be too high. T_e measurements, as well as the chemical composition of vent and pore fluids (see below), suggests that the fluids might best be modeled in the H_2O-NaCl-$CaCl_2$ system (Crawford, 1981; Vanko et al., 1988; Oakes et al., 1990), which has a eutectic temperature (T_e) of –52°C (Fig. 5). Recorded T_e temperatures below –52°C are likely due to the formation of metastable phases on freezing, as metastable melting events have been shown to be common at temperatures below –50°C (e.g., Vanko et al., 1988; Oakes et al., 1990; Davis et al., 1990).

Temperatures slightly lower than the eutectic are not thought to be due to the presence of other solutes such as Mg, which are known to further depress eutectic melting temperatures (Borisenko, 1977; Crawford et al., 1979). Basalt-seawater interaction experiments indicate low Mg concentrations of hydrothermal fluids at high temperatures (Mottl et al., 1979; Seyfried and Bischoff, 1981), and undiluted endmember fluids from active hydrothermal vents on the seafloor are essentially

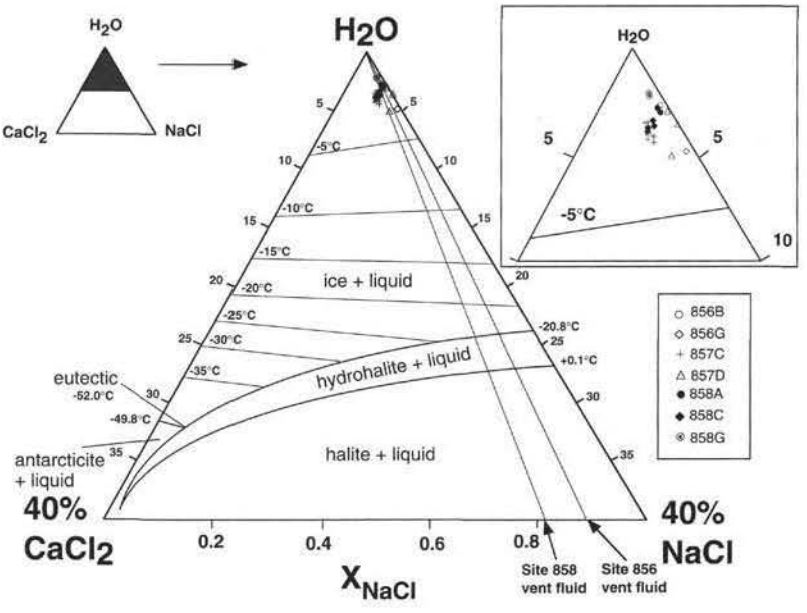

Figure 5. Ternary plot of phase relations in the H_2O-NaCl-$CaCl_2$ system. Isotherms in the ice + liquid field are plotted from data of Oakes et al. (1990). Cotectic boundaries are from Yanatieva (1946). Shown are NaCl/($CaCl_2$ + NaCl) weight fractions for fluid inclusions obtained from final hydrohalite melting temperatures in aqueous solutions and for vent fluids from Sites 858 and 856. Inset shows enlargement of H_2O apex.

devoid of Mg (less than 1 mmol/kg) as a result of extensive cation exchange between seawater and rocks in the subsurface within the downgoing (recharge) portions of the convective system (e.g., Von Damm, 1990). MV hydrothermal fluids that approach endmember compositions have only 3–6 mmol/kg Mg (Lydon et al., 1990, 1991, 1992; J.W. Lydon, unpubl. data), and endmember fluids have: 40–81 mmol/kg Ca, 315–398 mmol/kg Na, 13.5–18.7 mmol/kg K, 10–20 µmol/kg Fe, 63–78 µmol/kg Mn, and 412–578 mmol/kg Cl (Butterfield et al., this volume).

With continued slow heating, two fine-grained solid phases were visible in very few of the inclusions at low temperatures, and it was possible to measure the melting point of each of these. In order to obtain information on the relative contents of Na, Ca, and H_2O in the inclusion fluids, the sequential freezing method outlined in Haynes (1985) was used on selected, larger (15 to 70 µm diameter) inclusions. This technique involves the recooling of partly melted fluid inclusions and allowed the formation of hydrohalite ($NaCl.2H_2O$) (which possesses a refractive index greater than ice) and ice, and the unimpeded observation of hydrohalite melting (Thh) which occurred between –26.2° and –20.8°C (Fig. 4B). This allowed for the unambiguous observation of eutectic and cotectic phase equilibria (intermediate melting events) which could otherwise only rarely be observed.

Final melting of ice (T_m) occurred between –5.9° and –1.1°C (mean = –2.7° ± 1.0°C; n = 42) (Table 2). No evidence of clathrate melting was observed in any of the inclusions. Salinities were calculated from the temperature of final ice disappearance (freezing point depression) using the revised equation of Bodnar (1993). The temperatures of final ice melting correspond to salinities of 1.9 to 9.1 eq. wt% NaCl (mean = 4.3 ± 1.4 eq. wt% NaCl; n = 42) (Table 2; Fig. 6). Variations in T_m of low-salinity inclusions can result from differences in their gas contents because dissolved gases will also affect the freezing point depression (Hedenquist and Henley, 1985). There is a freezing point depression of 1.86°C per mole of CO_2, and because CO_2 clathrate is difficult to nucleate at low gas concentrations, the presence of CO_2 may go undetected (Moore et al., 1992). However, crushing studies of several inclusions did not indicate pressures greater than atmospheric, and significant CO_2 contents are not expected.

For inclusions where both T_{hh} and T_m data have been obtained, the relative ratios of Na to Ca in the inclusion fluids can be estimated (Table 2). The temperature at which hydrohalite melts defines the point at which the liquid composition leaves the cotectic and, therefore, constrains its relative Na/Ca ratio. On further heating the liquid

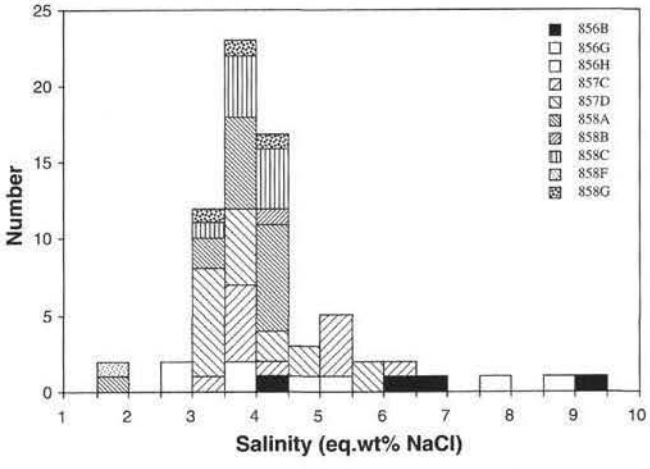

Figure 6. Frequency histogram of fluid inclusion salinities by drill hole.

composition moves toward the H_2O apex (Fig. 5), and the final melting of ice determines the point at which the liquid composition leaves the liquidus and hence fixes its bulk composition. Compositions for inclusion fluids from different sites are shown in Figure 5.

Because necking can alter the volumes and masses of fluid within inclusions (e.g., Sterner and Bodnar, 1989), only microthermometric data for inclusions which showed consistent liquid to vapor ratios are presented. We are aware of the possible stretching of inclusions in minerals such as anhydrite and sphalerite during microthermometric examination (e.g., Bodnar and Bethke, 1984). However, the T_t obtained for these minerals are similar to, or within the range determined for, other minerals such as quartz that are less susceptible to stretching, and on this basis we conclude that stretching problems were not important in this study.

Homogenization temperatures for all inclusions from all sites range from 58° to 330°C (mean = 219° ± 58°C [1σ]; n = 202). To obtain T_t, homogenization temperatures were corrected for the effect of pressure of the overlying water and sediment column. Because the pressure-volume-temperature properties for the H_2O-NaCl-$CaCl_2$ system are not available, pressure corrections were made using the properties for the NaCl-H_2O system (Potter, 1977). Potter and Brown (1977) have

Table 2. Microthermometric data from fluid inclusions in hydrothermal precipitates from MV samples and $NaCl/CaCl_2$ weight ratios calculated from available analyses of pore fluids extracted from nearest the fluid inclusion sample (Davis, Mottl, Fisher, et al., 1992).

Chip/inclusion	T_t (°C)	T_e (°C)	T_{hh} (°C)	T_m (°C)	Salinity (eq. wt% NaCl)	Fluid inclusion $NaCl/CaCl_2$ weight ratio	Pore fluid $NaCl/CaCl_2$ weight ratio
Sample 139-856B-15X-2, 67–69 cm (depth: 2532.6 mbsl; host mineral: quartz)							
1/1	208						
2/1	338						
2/2	234						
2/3	233						
3/1	193						
4/1	235	–47.6	–21.2	–2.4	4.0	6.5	28.7[a]
5/1	303						
5/2	217						
6/1	310						
7/1	181						
7/3	293						
8/1	294						
8/2	298						
8/3	252						
11/1	261						
11/2	255			–4.1	6.6		
12/1	303						
12/2	320						
12/3	276						
12/4	267						
12/5	270						
3/1	241	–45.9		–4.0	6.4		
14/1			–5.9	9.1			
Sample 139-856F-2X-CC, 23–25 cm (depth: 2435.2 mbsl; host mineral: dolomite)							
1/1	196						
1/2	204						
2/1	231						
2/2	242						
3/1	226						
3/2	218						
Sample 139-856G-7R-4, 4–6 cm (depth: 2422.8 mbsl; host mineral: sphalerite)							
2/1				–5.0	7.9		
6/1	260						
6/1	260						
7/1	253						
8/1	266						
9/1	241						
9/2				–2.2	3.7		
9/3		–45.5	–22.6	–3.2	5.3	5.6	NA
9/4				–2.2	3.7		
9/5	277						
9/6	278						
9/7	267						
9/8	262						
9/9	276						
10/1	259						
10/2	209						
Sample 139-856H-3R-2, 16–18 cm (depth: 2447.2 mbsl; host mineral: dolomite)							
1/1	207						
2/1	171						
3/1	161						
6/1	154						
6/2	158						
Sample 139-856H-3R-2, 84–87 cm (depth: 2447.9 mbsl; host mineral: dolomite)							
1/1	172						
2/1	164						
2/2	169			–5.5	8.5		
3/1	176	–56.0		–1.7	2.9		
3/2	198			–1.6	2.7		
5/1	174						
5/2	185	–46.3		–2.8	4.6		
5/3	169						
Sample 139-857C-60R-2, 28–30 cm (depth: 2904.2 mbsl; host mineral: quartz)							
1/1		–49.5		–1.8	3.1		
1/2				–2.1	3.5		
1/3		–50.6					
Sample 139-857C-61R-2, 4–6 cm (depth: 2913.6 mbsl; host mineral: quartz)							
1/1	268						
1/2	263						
1/3	244						
1/4	244						
Sample 139-857C-62R-1, 67–69 cm (depth: 2922.4 mbsl; host mineral: quartz)							
1/1	269						
1/2	278						
2/3	269						
3/1	258						
3/3	262						
3/4	277						
3/5	271						
3/6	268						
3/7	268						
3/8	269						
4/1	258						
4/2	275						
4/3	273						
4/4	269						
4/5	272						
4/6	272						
4/7	275						
Sample 139-857C-64R-2, 74–76 cm (depth: 2943.3 mbsl; host mineral: wairakite)							
1/1	273		–25.1	–2.2	3.7	2.9	2.7[b]
1/2	274			–2.2	3.7		
1/3			–24.9	–2.4	4.0	2.4	2.7[b]
1/4			–24.9	–2.2	3.7	2.4	2.7[b]
1/5	299		–25.1	–2.2	3.7	2.9	2.7[b]
3/1	261		–25.3	–3.0	5.0	3.0	2.7[b]
3/2	210			–3.9	6.3		
3/3				–3.2	5.3		
3/4	268		–25.1	–3.0	5.0	2.9	2.7[b]
3/5	268		–25.1	–3.0	5.0	2.9	2.7[b]
3/7	306						
Sample 139-857D-1R-1, 137–139 cm (depth: 3003.6 mbsl; host mineral: quartz)							
1/1	273						
1/2	267						
1/3	273						
2/1	272						
2/2	268						
2/3	278						
2/4	272						
2/5	270						
2/6	268						
2/7	268						
Sample 139-857D-11R-1, 1–3 cm (depth: 3100.6 mbsl; host mineral: quartz)							
2/1	276						
2/2	278						
2/3	248						
2/4	271						
2/5	250						
2/6	256						
2/7	258						
2/8	254						
2/9	267						
2/10	267						
2/11	278						
2/12	285						
2/13	249						
2/14	280						
2/15	259						
2/16	271						
2/17	268						
2/18	255						
2/19	270						
2/20	281						
2/21	268						
2/22	278						
2/23	269			–2.2	3.7		
2/24	264			–3.5	5.7		
2/25			–46.5	–1.8	3.1		
2/26			–48.8	–1.8	3.1		
2/27			–48.1	–1.8	3.1		
Sample 139-857D-12R-1, 88–90 cm (depth: 3107.4 mbsl; host mineral: wairakite)							
3/9				–2.8	4.6		
3/10			–56.4	–2.8	4.6		
4/5	311						
4/8	294						

Table 2 (continued).

Chip/inclusion	T_t (°C)	T_e (°C)	T_{hh} (°C)	T_m (°C)	Salinity (eq. wt% NaCl)	Fluid inclusion $NaCl/CaCl_2$ weight ratio	Pore fluid $NaCl/CaCl_2$ weight ratio
4/10	307						
6/2	350						
6/3	314						
6/6	275						
7/1	292						
8/4	318	–47.2	–23.5	–3.4	5.6	3.3	6.6[c]
9/5	281						
10/1			–26.2	–2.6	4.3	1.5	6.6[c]
10/2			–22.9			4.5	6.6[c]
10/5				–2.2	3.7		
10/6				–2.0	3.4		
10/7				–2.2	3.7		
10/9				–2.0	3.4		
10/11	242						
10/12				–2.0	3.4		
11/1	283						
12/1		–50.2	–20.8	–2.5	4.2	100	6.6[c]
12/2		–50.6	–21.0	–2.2	3.7	7.0	6.6[c]
Sample 139-858A-28X-CC, 4–5 cm (depth: 2649.0 mbsl; host mineral: anhydrite)							
1/1	311						
1/2	255						
1/3	283						
1/4	251						
1/5	269						
Sample 139-858A-29X-1, 30–32 cm (depth: 2663.1 mbsl; host mineral: anhydrite)							
1/1	236						
1/2	255						
1/3	231						
1/4	264						
1/5	259						
1/6	230						
1/7	254						
1/8	257						
1/9	259						
2/1		–47.5	–22.2	–2.2	3.7	5.4	4.6[d]
3/1	265	–48.1	–22.3	–2.6	4.3	5.3	4.6[d]
Sample 139-858B-2H-3, 113–115 cm (depth: 2421.0 mbsl; host mineral: anhydrite)							
1/1	152			–2.6	4.3		
2/1	141						
2/2	139						
2/3	149						
2/4	137						
2/5	139						
3/1	167						
Sample 139-858B-2H-4, 43–45 cm (depth: 2423.0 mbsl; host mineral: anhydrite)							
1/1	138						
1/2	90						
1/3	135						
Sample 139-858C-3H-1, 78–81 cm (depth: 2430.7 mbsl; host mineral: calcite)							
1/1	204						
1/2	186						
2/1	298						
Sample 139-858C-3H-1, 145–150 cm (depth: 2431.3 mbsl; host mineral: calcite)							
1/1	137						
1/2	138						
1/3	138						
1/4	140						
1/5	112						
1/6	150						
2/1	134						
2/2	128						
2/3	134						
2/4	119						
Sample 139-858C-3H-2, 10–15 cm (depth: 2431.5 mbsl; host mineral: calcite)							
1/1	192						
2/1	165						
3/1	184						
3/2	175						
4/1	135						
5/1	137						
5/2	126						
5/3	146						
Sample 139-858C-3H-3, 22–24 cm (depth: 2433.1 mbsl; host mineral: calcite)							
1/1	236			–2.1	3.5		
1/2	235						
1/3	242			–2.0	3.4		
1/4	230						
1/5	230						
1/6	240						
1/7	227						
2/1	247			–2.6	4.3		
2/2	232						
2/3	233						
2/4	235			–2.1	3.5		
2/5	234		–24.1	–2.3	3.9	3.1	21.1[e]
2/6	233			–2.2	3.7		
3/1	232		–26.0	–2.4	4.0	2.2	21.1[e]
3/2	219		–26.0	–2.5	4.2	2.2	21.1[e]
3/3	218						
3/4	233						
4/1		–48.2	–23.9	–2.4	4.0	3.2	21.1[e]
Sample 139-858F-2R-CC, 8–11 cm (depth: 2452.1 mbsl; host mineral: wairakite)							
1/1	280						
1/2	283	–46.0	–21.9			6.0	5.1[f]
1/3	283						
1/4	274						
1/5	279						
1/6	288						
1/7	270						
1/8				–1.1	1.9		
Sample 139-858G-16R-1, 77–79 cm (depth: 2838.8 mbsl; host mineral: quartz)							
1/1	293		–22.7	–2.0	3.4	4.3	NA
1/2	316	–48.1	–22.3	–2.1	3.5	5.3	NA
1/3	285			–2.5	4.2		
1/4	287						
1/5		–47.1					
1/6	250						

Note: NA = not analyzed.
[a] Calculated from sample IW-20.
[b] Calculated from sample IW-3.
[c] Calculated from sample G-5.
[d] Calculated from sample IW-23.
[e] Calculated from sample IW-6.
[f] Calculated from sample IW-1.

shown that the errors resulting from this approximation are very small. A correction ranging between 10° and 36°C for a 5 eq. wt% NaCl solution must be added to the homogenization temperatures, assuming hydrostatic conditions for the samples which were collected at depths between 2421.0 and 3107.4 mbsl. Calculated T_t for inclusions from all sites range between 90° and 350°C (mean = 240° ± 52°C [1σ]; n = 202) (Fig. 7A). There is a bimodal distribution of T_t (Fig. 7A). The lower temperature group represents inclusions in carbonate concretions and anhydrite from the low-temperature alteration zones and from dolomite interstitial to massive sulfide, and the higher temperature group is from inclusions in minerals co-precipitated with sulfides and/or from the high-temperature upflow zones (see Goodfellow and Peter, this volume). Fig. 7B–D gives frequency distributions of T_t for Sites 856, 857, and 858, respectively.

DISCUSSION

Comparison of Fluid Inclusion Data With Presently Venting Fluids and Pore Fluids

Temperature

For Site 858 (AAV), fluid inclusions in minerals from the high-temperature alteration zone (Fig. 7D) have T_t between about 220° and 316°C, which are in general agreement with venting hydrothermal fluids (184° and 276°C) measured with *ALVIN's* thermocouple probe (Goodfellow et al., 1994). At Site 857, T_t range between 210° and 350°C and have a mean of 272° ± 19°C (1σ). This mean temperature is very similar to the maximum measured temperature of 276°C for vent fluids from Site 858, supporting the interpretation that the hydro-

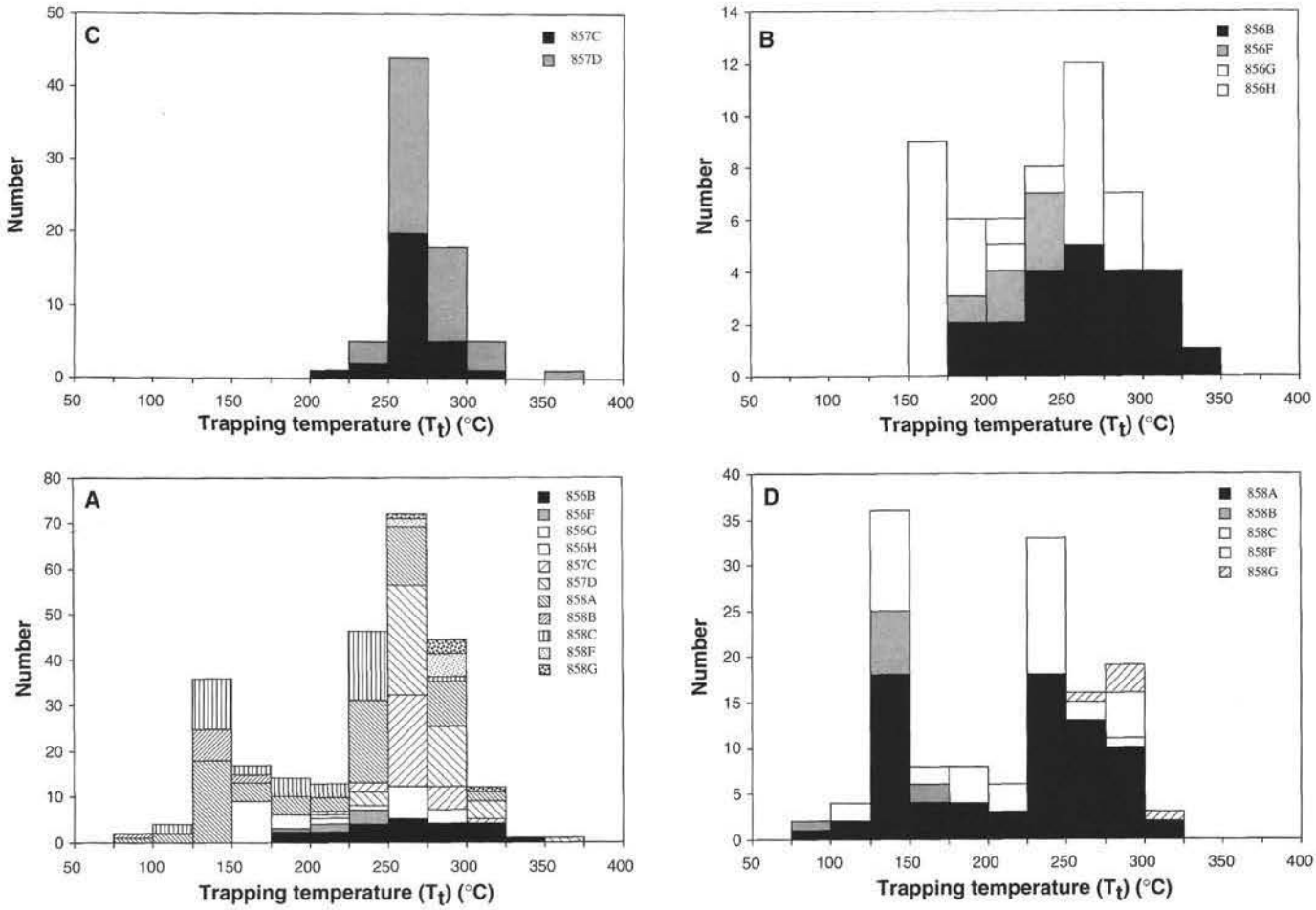

Figure 7. Frequency histograms of fluid inclusion trapping temperature by drill holes. **A.** All data from all sites. **B.** Holes 856B, -G, and -H. **C.** Holes 857C and -D. **D.** Holes 858A–F.

thermal fluids at Sites 857 and 858 are part of one hydrothermal circulation system, based on geochemical (Goodfellow and Peter, this volume) and mineralogical (Leybourne and Goodfellow, this volume) considerations. The majority of fluid inclusion temperature measurements in wairakite from Holes 857C, 857D, and 858F are well above 260°C (Table 2) and are within the stability field for wairakite and above the temperature at which laumontite reversibly dehydrates to form wairakite (231°C at 500 bars pH_2O; Liou, 1971).

T_t in quartz from the high-temperature alteration zone (Goodfellow and Peter, this volume) at Site 856 range up to 338°C. Massive sulfides from Site 856 are predominantly composed of pyrite, pyrrhotite, sphalerite, chalcopyrite/isocubanite, and magnetite. Although sphalerite is dominantly high-Fe (Goodfellow and Franklin, in press; Zierenberg, this volume) and unsuitable for fluid inclusion studies due to its opacity, T_t obtained from late-stage, low-Fe sphalerite range between 209° and 278°C. The higher temperatures obtained for the quartz indicate that this mineral may have been precipitated with main stage sulfides, whereas the lower temperature sphalerite likely was precipitated during the waning stages of hydrothermal circulation, and these inclusions may record an overprinting of the originally deposited high-temperature sulfide assemblage at Site 856. The temperatures obtained from the sphalerite span the 264°C measured temperature of fluids actively venting from anhydrite chimneys about 330 m south of the southern flank of BH (Fig. 2; Davis, Mottl, Fisher, et al., 1992) and T_t of 265°C obtained from anhydrite in chimneys from this site (Leitch, 1991). Therefore, the inclusions in the low-Fe sphalerite may have trapped similar fluids to those now venting at Sites 858 and 856.

Salinity

Salinities of vent fluids and pore fluids were calculated from the data of Butterfield et al. (this volume) using the empirical relation between salinity (S) and chlorinity (Cl): S (‰) = 0.03 + 1.805 Cl (‰) (Gerard, 1966). The average calculated salinity for Site 858 vent fluids (3.7 eq. wt% NaCl) is greater than normal MV bottom seawater (3.55 eq. wt% NaCl; Davis, Mottl, Fisher, et al., 1992, p. 198). For Site 856 vent fluids, the calculated salinity of 2.6 eq. wt% NaCl is below normal bottom seawater. Calculated pore fluid salinities from all sites range between 3.4 and 3.9 eq. wt% NaCl and are similar to normal MV bottom seawater, although they range to higher values. Most fluid inclusion salinities are between 2.5 and 5.5 eq. wt% NaCl (Fig. 6), and are in general agreement with the calculated salinities for vent fluids from Sites 858 and 856, pore fluid, and ambient bottom seawater. There is no observable relationship between salinity and depth, between T_t and salinity, or between T_e and T_t, which would suggest mixing between a low-salinity fluid (modified seawater) and a highly saline magmatic fluid (e.g., Shinohara et al., 1984, 1989). Salinities greater than seawater may result from the reaction of circulating seawater with subsurface sediments and the formation of hydrated clays and chlorite, where the salinity of the residual fluid is increased over seawater.

Cation Content and Ca Enrichment

Because Na and Ca are the only major cations in the vent fluids (Fe and Mn are insignificant: Fe = 10 to 20 µmol/kg and Mn = 63 to 78 µmol/kg; Butterfield et al., this volume), it is appropriate to compare the $NaCl/CaCl_2$ ratios of the vent fluids with those inferred for the fluid inclusions. Inclusion fluid $NaCl/CaCl_2$ weight ratios estimated from Figure 5 are 5.3 and 5.4 for Hole 858A; 2.2 and 3.2 in Hole 858C; 6.0 for Hole 858F; 4.3 and 5.3 for Hole 858G; between 2.4 and 3.0 for Hole 857C; between 1.5 and 7.0 (except for one high value) for Hole 857D; 6.5 for Hole 856B; and 5.6 for Hole 856G (Table 2). $NaCl/CaCl_2$ weight ratios for endmember vent fluids from MV (i.e., fluids in which the effects of admixed seawater have been removed by extrapolating to zero Mg content) are similar (Site 858: Na = 398 mmol/kg and Ca = 81 mmol/kg, giving a ratio of 4.5; Site 856: Na = 315 mmol/kg and Ca = 40 mmol/kg, giving a ratio of 7.2) to those estimated from fluid inclusions and the ratio for MV bottom seawater (41.8; calculated from Davis, Mottl, Fisher, et al., 1992, p. 198–199) and, except for several samples, MV pore fluids calculated from analyses in Davis, Mottl, Fisher, et al. (1992) for fluid nearest the fluid inclusion sample (1.5 to 7.0; Table 2). The similarity of the ratios for the inclusion fluids and vent and pore fluids indicates negligible variation in Ca and Na contents of the hydrothermal fluids at least since the precipitation of most sulfides to the present.

For comparison, the $NaCl/CaCl_2$ weight ratios for endmember hydrothermal fluids from Guaymas Basin, a sedimented rift hydrothermal site in the Gulf of California (Peter and Scott, 1988; Peter and Scott, 1991), are higher than MV vent fluids (11.4 to 16.4) but are low compared to seawater (Von Damm and Bischoff, 1987). However, the $NaCl/CaCl_2$ weight ratios for endmember hydrothermal fluids from nonsedimented sites are similar to those from MV: 7.2 to 9.3 for southern Juan de Fuca Ridge (calculated from Von Damm and Bischoff, 1987) and 9.5 to 10.0 for 13°N East Pacific Rise (EPR) (calculated from Michard et al., 1984). EPR endmember fluids from the nonsedimented site at 21°N are, however, much higher than those from MV (22.6 to 34.9; calculated from Von Damm et al., 1985). Thus, MV inclusions are relatively more Ca-rich than modern black smoker fluids from all measured vent fluids.

Basalts have been shown to constitute a source for Ca^{2+} to the interstitial pore fluids of the overlying sediments at certain seafloor hydrothermal systems (e.g., Lawrence et al., 1975; Gieskes and Lawrence, 1981; Lawrence and Gieskes, 1981). Vanko et al. (1992) proposed that the Ca contents of inclusion fluids in plutonic rocks from the Mid-Atlantic Ridge were modified by the albitization of plagioclase at greenschist facies conditions at very low water/rock ratios (w/r). Such a process may also explain the higher Ca contents of the MV inclusion fluids whereby plagioclase in the subsurface sediments are albitized to produce Ca-enriched, Mg-depleted, low-pH fluids capable of precipitating epidote and wairakite. Indeed, Leybourne and Goodfellow (this volume) show that significant albitization of plagioclase has occurred in the altered sediments, and Goodfellow and Peter (this volume) point out the high-Ca activity of the fluids at AAV, based on thermochemical modeling of the fluid compositions. Although there are only limited data for inclusions from Site 856, these inclusion fluids (and vent fluids) appear to be less calcic than those from Sites 858 and 857 (Fig. 5), and this may be due to differing w/r between these sites.

Comparison of Fluid Inclusion Data from Sites 856, 857, and 858

T_t for Site 857 (210° to 350°C; mean = 272° ± 19°C [1σ]; n = 74) and for high-temperature inclusions from Site 858 (218° to 316°C; mean = 255° ± 25°C [1σ]; n = 44) are similar. Fluid inclusion salinities from the high-temperature population at Site 858 (1.9 to 4.3 eq. wt% NaCl; mean = 3.7 ± 0.6 eq. wt% NaCl [1σ]; n = 15) are within the range of inclusion salinities from Site 857, although the latter extend to higher salinities (3.1 to 6.3 eq. wt% NaCl; mean = 4.1 ± 0.9 eq. wt% NaCl [1σ]; n = 28). These similarities suggest a common origin for the fluids at these two sites, a conclusion also supported by the similarities between the high temperature alteration mineralogy of these two sites (Leybourne and Goodfellow, this volume) and by location of these sites along the same axis-parallel thermal anomaly (Davis and Villinger, 1992). The slightly higher mean temperature and salinity for Site 857 may indicate that the fluids at this site have mixed less with seawater and more closely approach endmember compositions. This is consistent with the more Ca-rich chemistry of wairakite at Site 857 (Leybourne and Goodfellow, this volume). T_t for quartz and sphalerite at Site 856 (Fig. 7B) are similar to temperatures from Sites 857 and 858. Salinities from Site 856 (2.7 to 9.1 eq. wt% NaCl; mean = 5.5 ± 2.2 eq. wt% NaCl [1θ]; n = 12) are slightly higher than those for Sites 857 and 858; however, these fluid inclusion data for authigenic quartz at Site 856 are from a mineral which may be cogenetic with main-stage sulfide deposition, whereas fluid inclusion data from dolomite and low-iron sphalerite likely represent later, lower temperature fluids perhaps similar to those presently venting at Site 858.

Relationship Between Fluid Inclusion Temperatures and Depth

For all sites, there is a general trend of increasing minimum T_t with increasing sample depth of about 9°C per 100 m (Fig. 8). Such a trend is not due solely to a normal geothermal gradient. Figure 8 shows that for all sites, there is a relatively constant maximum temperature of around 320°C. Furthermore, below about 2650 mbsl inclusions have a relatively consistent minimum temperature of around 230° to 240°C. This indicates that within the core of the upflow zone, endmember fluids were heated to a temperature of around 320°C by cooling subsurface magmatic sills and/or other intrusive bodies before buoyantly traveling to the seafloor. Cold seawater is drawn down into the subsurface and mixes with the endmember fluids, thereby reducing the temperature of the mixture. This temperature reduction is greatest nearest the seafloor and decreases consistently to a maximum depth of around 2650 mbsl. Below this depth, significantly less seawater mixes with the endmember fluids. For these samples, lower temperatures may have resulted from conductive cooling and adiabatic expansion in addition to entrainment of seawater. Maximum fluid inclusion temperatures of around 320°C at Site 857 are slightly higher than the calculated maximum value of 280°C of Davis and Wang (this volume). These authors indicate that temperatures were never higher than those presently venting; however, fluid inclusions indicate that fluids were hotter in the past than those presently venting in MV by about 40°C.

Carbon and Oxygen Isotope Composition of Hydrothermal Fluid

Baker et al. (this volume) present carbon and oxygen isotope data for hydrothermal carbonates from MV, and these data are not discussed in detail here. However, the combined use of T_t obtained from fluid inclusions for dolomite and calcite, and carbon and oxygen isotope compositions of those same samples, allows the calculation of the carbon and oxygen isotope compositions of hydrothermal fluid from which the carbonates precipitated, assuming equilibrium conditions between the fluid and the precipitated mineral prevailed. Three of the samples for which isotopic measurements were made were hand-picked from calcite crystals adjacent to crystals from which fluid inclusion measurements were made. For the other three, isotopic measurements were made from bulk samples (Table 1). However, there may be some error introduced for these latter samples because some of the carbonate concretions at MV are isotopically zoned (Al-Aasm and Blaise, 1991; Goodfellow et al., 1994). The MV vent fluids from Sites 858 and 856 have estimated pH values of 5.5 and 5.1, respectively (Butterfield et al., this volume), which limits the dominant carbon species in solution to CO_2 and H_2CO_3. Carbon isotope fractionations in systems containing H_2CO_3 are unknown, but at

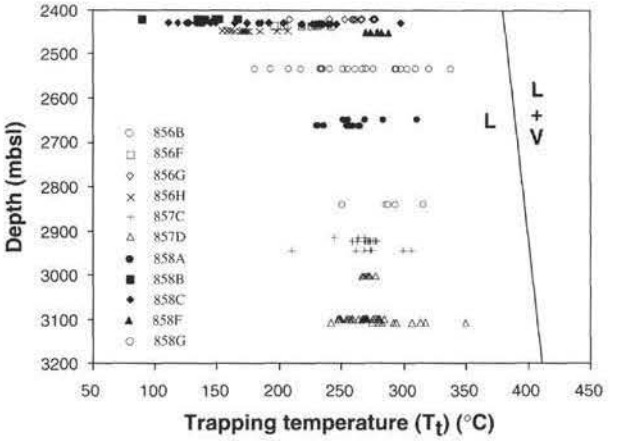

Figure 8. Fluid inclusion trapping temperature vs. sample depth (by drill hole). Liquid (L)–vapor (V) coexistence curve shown (from Bischoff and Pitzer, 1985) is for a fluid of seawater salinity.

temperatures above 100°C, H_2CO_3 in solution may be isotopically approximated by CO_2 gas (Ohmoto, 1972). Therefore, calcite-CO_2 and dolomite-CO_2 fractionation can be used to investigate the initial carbon isotopic composition of the hydrothermal fluid.

The $\delta^{13}C$ composition of the fluid was determined from calcite data using the expression of Bottinga (1969):

$$1000ln\alpha_{\text{calcite-CO}_2} = -8.914/T^3 \times 10^8 + 8.557/T^2 \times 10^6 - 18.11/T \times 10^3 + 8.27. \quad (1)$$

The $\delta^{13}C$ composition of the fluid was determined from dolomite data using the expression given in Ohmoto and Rye (1979), which was calculated using the equilibrium isotopic fractionation factor for dolomite and carbon dioxide of Sheppard and Schwarcz (1970):

$$1000ln\alpha_{\text{dolomite-CO}_2} = -8.914/T^3 \times 10^8 + 8.737/T^2 \times 10^6 - 18.11/T \times 10^3 + 8.44. \quad (2)$$

Calculated carbon isotope compositions for the fluids range between –35.4‰ and –7.0‰ (Table 3) and are similar to measured vent fluid $\delta^{13}C$ compositions, which range between –32.98‰ and –10.64‰ (Taylor, 1990). These light compositions have been explained by Goodfellow et al. (1994) to result from the oxidation of hydrothermally derived methane by sulfate-reducing bacteria, as proposed by Reeburgh (1980), where methane is oxidized either thermogenically within the sedimentary pile or biogenically at the seafloor.

Oxygen isotope compositions of fluid from which calcite was precipitated were calculated using the fractionation factor for the calcite-water system determined experimentally by O'Neil et al. (1969) combined with the CO_2-H_2O fractionation factor at 25°C ($\alpha = 1.0412$; O'Neil et al., 1975). This results in the following expression of Friedman and O'Neil (1977):

$$1000ln\alpha_{\text{calcite-water}} = 2.78\ (10^6T^{-2}) - 2.89, \quad (3)$$

where T is in Kelvin. Oxygen isotope compositions of fluid from which dolomite was precipitated were calculated using the experimentally determined fractionation expression for the dolomite-water system of Northrop and Clayton (1966):

$$1000ln\alpha_{\text{dolomite-water}} = 3.20(10^6T^{-2}) - 1.50, \quad (4)$$

where T is in Kelvin. Rather than using this dolomite-water fractionation curve, we could have used the curves of Land (1980, 1985). Although these alternate equations produce slightly different $\delta^{18}O$ values for the fluid, the differences are insufficient to alter the conclusions reached. Descriptions of the samples used, and the estimated oxygen and carbon isotope compositions of the hydrothermal fluid, are listed in Table 3.

Sample 139-858C-3H-3, 22–24 cm, the highest temperature sample for which isotope data was obtained, gives an estimated fluid composition ($\delta^{18}O = +0.4$‰) that is similar to fluids sampled to date from modern hydrothermal black smokers. Craig et al. (1980) reported the oxygen isotope composition of one vent fluid sample from 21°N, EPR at +1.6‰; a revised value for the fluid was given by Bowers and Taylor (1985; +2.5‰). Merlivat et al. (1987) report $\delta^{18}O$ values from 13°N, EPR, of +0.39‰ to +0.69‰. Brines from the Red Sea have $\delta^{18}O$ values of +1‰ to +2‰ (Craig, 1969). The fluid compositions calculated for calcite from carbonate concretions (Samples 858C-3H-1, 145–150 cm, and 858C-3H-2, 10–15 cm) are significantly enriched in ^{18}O (+11.7‰ and +9.3‰), in comparison to modern high-temperature hydrothermal fluids. One sample of calcite from calcite-pyrite veins which cross-cut sediment gives a fluid composition of +18.6‰. Two samples of dolomite, which fills interstices in sulfides, have fluid compositions of +3.2‰ and +4.2‰, which are less enriched than the concretions but are still more enriched than modern hydrothermal vent fluids.

Several possible mechanisms can explain high-^{18}O fluids: (1) mixing with juvenile, magmatic fluids; (2) high-temperature interaction of seawater with rocks at low w/r (Ohmoto and Rye, 1974; Pisutha-Arnond and Ohmoto, 1983; Bowers and Taylor, 1985); (3) exchange with ^{18}O-enriched volcanic and/or sedimentary rocks (Barriga and Kerrich, 1984); (4) enrichment by ultra-filtration. In ultrafiltration, water circulating through clay or shale undergoes isotopic fractionation, and the residual water is enriched in ^{18}O over the starting water and ultrafiltrate (Coplen and Hanshaw, 1973). However, this process only enriches the residual fluid in the heavy isotope by less than 1‰ and cannot, therefore, explain the heavy values obtained in this study. Although interaction with basaltic rocks likely affected the oxygen isotope composition of the fluids significantly, the fluids are even more ^{18}O-enriched than waters in equilibrium with normal mafic magmas (6‰ ± 0.5‰) and juvenile waters (6‰ ± 1‰) (Taylor, 1979) and, therefore, must have also undergone isotopic exchange with sediments.

Thus, the most plausible explanation for the ^{18}O-enriched nature of the MV hydrothermal fluids is that they have interacted with sediments rich in authigenic silicate phases that are enriched in ^{18}O in the subsurface. Most clay minerals have $\delta^{18}O$ values typically between +15‰ and +30‰ (e.g., Hoefs, 1980; Savin and Epstein, 1970a, 1970b; Lawrence and Taylor, 1971, 1972). Oxygen isotope analyses of two samples of unaltered hemipelagic sediment from MV give $\delta^{18}O$ compositions of +10.9‰ and +11.7‰ (Goodfellow et al., 1994) and fall within the range of +9‰ to +13‰ for ocean sediments on a carbonate-free basis (Savin and Epstein, 1970b). Formation waters are typically ^{18}O-enriched from exchange with subsurface sediments (Clayton et al., 1966; Hitchon and Friedman, 1969; Kharaka et al., 1973).

Goodfellow et al. (in press) used the oxygen isotope compositions of carbonate concretions to calculate precipitation temperatures in the range of 60° to 100°C by assuming $\delta^{18}O$ values of 0‰ for the fluid. Baker et al. (this volume) used the same technique to calculate maximum temperatures for carbonates in ODP cores from MV in the range of 165° to 222°C. However, our data are considerably more complex and show variable enrichments of the MV hydrothermal fluids in ^{18}O which are likely a result of interaction with subsurface sediments at variable w/r. Thus, temperatures for carbonate precipitation calculated assuming the fluid has a $\delta^{18}O$ composition of 0‰ may be too low.

CONCLUSIONS

Fluid inclusion studies of hydrothermal precipitates in Hole 858C in MV indicate carbonate concretions in the outer low-temperature alteration zone formed at temperatures between 112° and 192°C. Hydrothermal minerals were precipitated near the core of the upflow

Table 3. Carbon and oxygen isotope compositions of calcite and dolomite, and calculated carbon and oxygen isotope compositions of hydrothermal fluid in equilibrium with these minerals. See text for details of calculations.

Sample Number	Sample Type	Mean T_t (± 1 σ °C)	$\delta^{18}O_{SMOW}$ carbonate (‰)	$\delta^{18}O_{SMOW}$ fluid (‰)*	$\delta^{13}C_{PDB}$ carbonate (‰)	$\delta^{13}C_{PDB}$ fluid (‰)§
856F-2X-CC, 23-25 cm	bulk dolomite matrix with sulfide clasts & indurated sediment	220 ± 17 (n=6)	+14.8#	+3.2	-15.5#	-15.7
856H-3R-2, 16-18 cm	bulk dolomite matrix interstitial to sulfides	170 ± 21 (n=5)	+18.9#	+4.2	-5.2#	-7.0
858C-3H-1, 78-81 cm	bulk calcite from calcite-pyrite veins cutting sediment	195 ± 13 (n=2)	+28.4#	+18.6	-33.9#	-33.9
858C-3H-1, 145-150 cm	hand-picked calcite crystals from calcite concretion	133 ± 10 (n=10)	+23.2	+9.3	-33.1	-35.4
858C-3H-2, 10-15 cm	hand-picked calcite crystals from calcite concretion	158 ± 25 (n=8)	+25.3	+13.2	-29.6	-30.7
858C-3H-3, 22-24 cm	hand-picked calcite crystals in hydrothermally altered, calcite & sulfide-bearing sediment	233 ± 7 (n=17)	+8.3	+0.4	-21.0	-20.0

*oxygen isotope composition of fluid calculated using the mean fluid inclusion trapping temperature and either the calcite, the calcite-water equation of Friedman and O'Neil (1977), or the dolomite-water equation of Northrop and Clayton (1966), all of which assume equilibrium fractionation between the mineral and fluid.

§carbon isotope composition of fluid calculated using the mean fluid inclusion trapping temperature and either the calcite-CO_2 equation of Bottinga (1969) or the empirical fractionation factors between dolomite and calcite of Sheppard and Schwarcz (1970) which assume equilibrium fractionation between the mineral and fluid.

#from W. Goodfellow (unpubl. data).

zone at higher temperatures, between about 200°C and 350°C. These temperatures are similar to those for presently venting hydrothermal fluids. T_t and salinities for Site 857, and for high-temperature inclusions from Site 858 are similar and are consistent with a common origin for the fluids at these two sites. T_t for sphalerite at Site 856 are similar to temperatures from Sites 857 and 858; however, salinities from Site 856 are slightly higher. There is a general increase in minimum T_t with increasing depth due to conductive heating from cooling sills and/or intrusives and mixing with down-drawn cold seawater which cools fluids in the upper part of the upflow zone. Fluid inclusion microthermometric data indicate that Ca, Na, and Cl are the dominant ionic species, and the hydrothermal fluids are modified seawater. Salinities for most inclusion fluids range between 2.5 and 7.0 eq. wt% NaCl, and most are similar to ambient bottom water (≈3.2 wt%). Estimated carbon isotope compositions of the evolved hydrothermal fluids on the margin of fluid upflow ($\delta^{13}C$ = –7.0‰ to –35.4‰) are similar to presently venting hydrothermal fluids. Most estimated oxygen isotope compositions of these fluids are considerably enriched in ^{18}O (+3.2‰ to +18.6‰) compared to seawater and indicate significant isotopic exchange with sediments. Furthermore, the variability in calculated carbon and oxygen isotope compositions of hydrothermal fluids indicate complex spatial and possibly temporal variations in processes that fractionate these isotopes, and likely result from fluctuating water/rock ratios.

ACKNOWLEDGMENTS

We thank Jim Franklin for providing samples of veins within mafic sills for study and John Lydon for discussion. This work was performed while J.M. Peter held a Natural Sciences and Engineering Research Council of Canada Visiting Fellowship. We thank David A. Vanko and Craig H.B. Leitch for very thorough reviews. The incisive criticisms and comments of David Vanko were of particular help and greatly improved this paper. We also acknowledge the editorial comments of N. McQuistion. This is Geological Survey of Canada contribution no. 47392.

REFERENCES*

Barriga, F.J.A.S., and Kerrich, R., 1984. Extreme ^{18}O-enriched volcanics and ^{18}O-evolved marine water, Alujustrel, Iberian pyrite belt: transition from high to low Rayleigh number convective regimes. *Geochim. Cosmochim. Acta,* 48:1021–1031.

Bischoff, J.L., and Pitzer, K.S., 1985. Phase relations and adiabats in boiling seafloor geothermal systems. *Earth Planet. Sci. Lett.,* 75:327–338.

Bodnar, R.J., 1993. Revised equation and table for determining the freezing point depression of H_2O-NaCl solutions. *Geochim. Cosmochim. Acta,* 57:683–684.

Bodnar, R.J., and Bethke, P.M., 1984. Systematics of stretching of fluid inclusions, I: Fluorite and sphalerite at 1 atmosphere confining pressure. *Econ. Geol.,* 79:141–161.

Bodnar, R.J., Reynolds, T.J., and Kuehn, C.A., 1985. Fluid inclusion systematics in epithermal systems. *Rev. Econ. Geol.,* 2:73–98.

Borisenko, A.S., 1977. Study of the salt composition of solutions in gas-liquid inclusions in minerals by the cryometric method. *Sov. Geol. Geophys. Eng. Transl.,* 18:11–19.

Bottinga, Y., 1969. Calculated fractionation factors for carbon and hydrogen isotopic exchange in the system calcite-carbon dioxide-graphite, methane-hydrogen-water vapor. *Geochim. Cosmochim. Acta,* 33:49–64.

Bowers, T.S., and Taylor, H.P., Jr., 1985. An integrated chemical and stable isotope model of the origin of midocean ridge hot spring systems. *J. Geophys. Res.,* 90:12583–12606.

Clayton, R.N., Friedman, I., Graf, D.L., Mayeda, T.K., Meents, W.F., and Shimp, N.F., 1966. The origin of saline formation waters, I. Isotopic composition. *J. Geophys. Res.,* 71:3869–3882.

Coplen, T.B., and Hanshaw, B.D., 1973. Ultrafiltration by a compacted clay membrane, I. Oxygen and hydrogenisotopic fractionation. *Geochim. Cosmochim. Acta,* 37:2295–2310.

Craig, H., 1969. Geochemistry and origin of the Red Sea brines. *In* Degens, E.T., and Ross, D.A. (Eds.), *Hot Brines and Recent Heavy Metal Deposits in the Red Sea:* New York (Springer-Verlag), 208–242.

* Abbreviations for names of organizations and publications in ODP reference lists follow the style given in *Chemical Abstracts Service Source Index* (published by American Chemical Society).

Craig, H., Welhan, J.A., Kim, K., Poreda, R., and Lupton, J.E., 1980. Geochemical studies of the 21°N EPR hydrothermal fluids. *Eos,* 61:992.

Crawford, M.L., 1981. Phase equilibria in aqueous fluid inclusions. *Fluid Inclusions: Applications to Petrology.* Mineral. Assoc. Can., 75–100.

Crawford, M.L., Filer, J., and Wood, C., 1979. Saline fluid inclusions associated with retrograde metamorphism. *Bull. Mineral.,* 102:562–568.

Davis, D.W., Lowenstein, T.K., and Spencer, R.J., 1990. Melting behavior of fluid inclusions in laboratory-grown halite crystals in the systems NaCl-H_2O, NaCl-H_2O, NaCl-$MgCl_2$-H_2O, and NaCl-$CaCl_2$-H_2O. *Geochim. Cosmochim. Acta,* 54:91–601.

Davis, E.E., Goodfellow, W.D., Bornhold, B.D., Adshead, J., Blaise, B., Villinger, H., and Le Cheminant, G.M., 1987. Massive sulfides in a sedimented rift valley, northern Juan de Fuca Ridge. *Earth Planet. Sci. Lett.,* 82:49–61.

Davis, E.E., Mottl, M.J., Fisher, A.T., et al., 1992. *Proc. ODP, Init. Repts.,* 139: College Station, TX (Ocean Drilling Program).

Davis, E.E., and Sawyer, B., 1987. Marine geophysical maps of western Canada. Geol. Surv. Can. Bathymetric Map 6-1987.

Davis, E.E., and Villinger, H., 1992. Tectonic and thermal structure of the Middle Valley sedimented rift, northern Juan de Fuca Ridge. *In* Davis, E.E., Mottl, M.J., Fisher, A.T., et al., *Proc. ODP, Init. Repts.,* 139: College Station, TX (Ocean Drilling Program), 9–41.

Franklin, J.M., Goodfellow, W.D., Ames, D.E., Lydon, J.W., Jonasson, I.R., and Davis, E.E., 1991. Middle Valley, a major centre of hydrothermal activity in a sedimented ridge crest, northern Juan de Fuca Ridge. *Progr. with Abstr., Geol. Surv. Can., Curr. Activ. Forum, Ottawa,* 20.

Franklin, J.M., and Leg 139 Scientific Party, 1992. Formation of massive sulphide deposits in Middle Valley, northern Juan de Fuca Ridge. *Geol. Surv. Can. Minerals Colloq., Ottawa, Abstr. with Progr.,* 20.

Friedman, I., and O'Neil, J., 1977. Compilation of stable isotope fractionation factors of geochemical interest. *In* Fleischer, M. (Ed.), *Data of Geochemistry* (6th Ed.). Geol. Surv. Prof. Pap. U.S., 440-KK:1–12.

Gerard, R., 1966. Salinity in the ocean. *In The Encyclopedia of Oceanography:* Toronto (Van Nostrand Reinhold).

Gieskes, J.M., and Lawrence, J.R., 1981. Alteration of volcanic matter in deep-sea sediments: evidence from the chemical composition of interstitial waters from deep-sea drilling cores. *Geochim. Cosmochim. Acta,* 45:1687–1703.

Goodfellow, W.D., and Blaise, B., 1988. Sulfide formation and hydrothermal alteration of hemipelagic sediment in Middle Valley, northern Juan de Fuca Ridge. *Can. Mineral.,* 26:675–696.

Goodfellow, W.D., and Franklin, J.M., in press. Geology, mineralogy and geochemistry of massive sulfides in shallow cores, Middle Valley, Northern Juan de Fuca Ridge. *Econ. Geol.*

Goodfellow, W.D., Grapes, K., Cameron, B., and Franklin, J.M., 1994. Hydrothermal alteration associated with massive sulfide deposits, Middle Valley, Northern Juan de Fuca Ridge. *Can. Mineral.,* 31:1025–1060.

Hedenquist, J.W., and Henley, R.W., 1985. The importance of CO_2 on freezing point measurements of fluid inclusions: evidence from active geothermal systems and implications for epithermal ore deposition. *Econ. Geol.,* 80:1379–1406.

Hitchon, B., and Friedman, I., 1969. Geochemistry and origin of formation waters in the western Canada sedimentary basin. I. Stable isotopes of hydrogen and oxygen. *Geochim. Cosmochim. Acta,* 33:1321–1349.

Hoefs, J., 1980. *Stable Isotope Geochemistry* (2nd ed.): New York (Springer-Verlag).

Holland, R.A.G., Bray, C.J., and Spooner, E.T.C., 1978. A method for preparing thin sections suitable for microthermometric examination of fluid inclusions. *Mineral. Mag.,* 42:407–408.

Kharaka, Y.K., Berry, F.A.F., and Friedman, I., 1973. Isotopic composition of oil-field brines from Kettleman North Dome oil field, California, and their geologic implications. *Geochim. Cosmochim. Acta,* 37:1899–1908.

Land, L.S., 1980. The isotopic and trace element geochemistry of dolomite: the state of the art. *In* Zenger, D.H., Dunham, J.B., and Ethington, R.L. (Eds.), *Concepts and Models of Dolomitization.* Soc. Econ. Paleontol. Mineral. Pomona Coll., 87–110.

————, 1985. The origin of massive dolomite. *J. Geol. Educ.,* 33:112–125.

Lawrence, J.R., and Gieskes, J.M., 1981. Constraints on water transport and alteration in the oceanic crust from the isotopic composition of pore water. *J. Geophys. Res.,* 86:7924–7934.

Lawrence, J.R., Gieskes, J.M., and Broecker, W.S., 1975. Oxygen isotope and cation composition of DSDP pore water and the alteration of layer II basalts. *Earth Planet. Sci. Lett.,* 27:1–10.

Lawrence, J.R., and Taylor, H.P., 1972. Hydrogen and Oxygen isotope systematics in weathering profiles. *Geochim. Cosmochim. Acta,* 36:1377–1393.

Lawrence, J.R., and Taylor, H.P., Jr., 1971. Deuterium and oxygen-18 correlation: clay minerals and hydroxides in Quaternary soils compared to meteoric waters. *Geochim. Cosmochim. Acta,* 35:993–1003.

Leitch, C.H.B., 1991. Preliminary studies of fluid inclusions in barite from the Middle Valley sulphide mounds, northern Juan de Fuca Ridge. *Geol. Surv. Can. Curr. Res., Part A.,* 27–30.

Liou, J.G., 1971. Pressure-temperature stabilities of laumontite, wairakite, lawsonite, and related minerals in the system $CaAl_2Si_2O_8$-H_2O. *J. Petrol.,* 12:379–411.

Lydon, J.W., Goodfellow, W.D., and Franklin, J.M., 1990. Chemistry of sediment pore waters around active hydrothermal vents, Middle Valley. *Am. Geophys. Union, Annual Meeting Progr. Abstr.,* 71:1569.

————, 1991. Spatial control and pore water compositions of active and extinct hydrothermal fields in Middle Valley. *Int. Conf. on Fluids in Subduction Zones, Paris, France.*

Lydon, J.W., Goodfellow, W.D., and Gregoire, D.C., 1992. Chemical composition of vent and pore fluids in an active hydrothermal discharge zone, Middle Valley. *Geol. Surv. Can. Minerals Colloq., Progr. Abstr.,* 7.

McCrea, J.M., 1950. Isotopic chemistry of carbonates and a paleotemperature scale. *J. Chem. Phys.,* 18:849–857.

MacDonald, A.J., and Spooner, E.T.C., 1981. Calibration of a Linkam TH600 programmable heating-cooling stage for microthermometric examination of fluid inclusions. *Econ. Geol.,* 76:1248–1258.

Merlivat, L., Pineau, F., and Javoy, M., 1987. Hydrothermal vent waters at 13°N on the East Pacific Rise: isotopic composition and gas concentration. *Earth Planet. Sci. Lett.,* 84:100–108.

Michard, G., Albarede, F., Michard, A., Minster, J.-F., Charlou, J.-L., and Tan, N., 1984. Chemistry of solutions from 13°N East Pacific Rise hydrothermal site. *Earth Planet. Sci. Lett.,* 67:297–308.

Moore, J.N., Adams, M.C., and Lemieux, M.M., 1992. The formation and distribution of CO_2-enriched fluid inclusions in epithermal environments. *Geochim. Cosmochim. Acta,* 56:121–135.

Mottl, M.J., Holland, H.D., and Corr, R.F., 1979. Chemical exchange during hydrothermal alteration of basalt by seawater. II. Experimental results for Fe, Mn and sulfur species. *Geochim. Cosmochim. Acta,* 43:869–884.

Northrop, D.A., and Clayton, R.N., 1966. Oxygen-isotope fractionations in systems containing dolomite. *J. Geol.,* 74:174–196.

Oakes, C.S., Bodnar, R.J., and Simonson, J.M., 1990. The system NaCl-$CaCl_2$-H_2O, I. The ice liquidus at 1 atm total pressure. *Geochim. Cosmochim. Acta,* 54:603–610.

Ohmoto, H., 1972. Systematics of sulfur and carbon isotopes in hydrothermal ore deposits. *Econ. Geol.,* 67:551–579.

Ohmoto, H., and Rye, R.O., 1974. Hydrogen and oxygen isotopic compositions of fluid inclusions in the Kuroko deposits, Japan. *Econ. Geol.,* 69:947–953.

————, 1979. Isotopes of sulfur and carbon. *Geochemistry of Hydrothermal Ore Deposits* (2nd ed.): New York (Wiley), 509–567.

O'Neil, J.R., Adami, L.H., and Epstein, S., 1975. Revised value for the ^{18}O fractionation between CO_2 and H_2O at 25°C. *J. Res. U.S. Geol. Surv.,* 3:623–624.

O'Neil, J.R., Clayton, R.N., and Mayeda, T.K., 1969. Oxygen isotope fractionation in divalent metal carbonates. *J. Chem. Phys.,* 51:5547–5558.

Peter, J.M., and Scott, S.D., 1988. Mineralogy, composition, and fluid-inclusion microthermometry of seafloor hydrothermal deposits in the southern trough of Guaymas Basin, Gulf of California. *Can. Mineral.,* 26:567–587.

————, 1991. Hydrothermal mineralization in the Guaymas Basin, Gulf of California. *AAPG Mem.,* 47:721–741.

Pisutha-Arnond, V., and Ohmoto, H., 1983. Thermal history, and chemical and isotopic compositions of the ore-forming fluids responsible for the Kuroko massive sulfide deposits in the Hokuroku District of Japan. *Econ. Geol. Monogr.,* 5:523–558.

Potter, R.W., 1977. Pressure corrections for fluid-inclusion homogenization temperatures based on the volumetric properties of the system NaCl-H_2O. *J. Res. U.S. Geol. Surv.,* 5:603–607.

Potter, R.W., II, and Brown, D.L., 1977. The volumetric properties of aqueous sodium chloride solutions from 0°C to 500°C at pressures up to 2000 bars based on a regression of available data in the literature. *U.S. Geol. Surv. Bull.,* 1421-C:1–35.

Reeburgh, W.S., 1980. Anaerobic methane oxidation: rate depth distribution in Skan Bay sediments. *Earth Planet. Sci. Lett.,* 47:345–352.

Roedder, E., 1984. Fluid inclusions. *Rev. Mineral., Mineral. Soc. Am.,* 12.

Savin, S.M., and Epstein, S., 1970a. The oxygen and hydrogen isotope geochemistry of clay minerals. *Geochim. Cosmochim. Acta,* 34:25–42.

————, 1970b. The oxygen and hydrogen isotope geochemistry of ocean sediments and shales. *Geochim. Cosmochim. Acta,* 34:43–63.

Seyfried, W.E., Jr., and Bischoff, J.L., 1981. Experimental seawater-basalt interaction at 300°C and 500 bars: chemical exchange, secondary mineral formation, and implications for the transport of heavy metals. *Geochim. Cosmochim. Acta,* 45:135–1.

Shepherd, T.J., 1981. Temperature-programmable, heating-freezing stage for microthermometric analysis of fluid inclusions. *Econ. Geol.,* 76:1244–1247.

Sheppard, S.M.F., and Schwarz, H.P., 1970. Fractionation of carbon and oxygen isotopes and magnesium between metamorphic calcite and dolomite. *Contrib. Mineral. Petrol.,* 26:161–198.

Shinohara, H., Iiyama, J.T., and Matsuo, S., 1984. Geochemistry-behavior of chlorine in the system granitic magma-hydrothermal solution. *C.R. Acad. Sci. Ser. 2,* 298:741–743. (in French)

————, 1989. Partition of chlorine compounds between silicate melt and hydrothermal solutions, I. Partition of NaCl-KCl. *Geochim. Cosmochim. Acta,* 53:2617–2630.

Simoneit, B.R.T., Goodfellow, W.D., and Franklin, J.M., 1992. Hydrothermal petroleum at the seafloor and organic matter alteration in sediments of Middle Valley, northern Juan de Fuca Ridge. *Appl. Geochem.,* 7:257–264.

Sterner, S.M., and Bodnar, R.J., 1989. Synthetic fluid inclusions, VII. Re-equilibration of fluid inclusions in quartz during laboratory-simulated metamorphic burial and uplift. *J. Metamorph. Geol.,* 7:243–260.

Taylor, B.E., 1990. Carbon dioxide and methane in hydrothermal vent fluids from Middle Valley, a sediment-covered ridge segment. *Eos,* 71:1569.

Taylor, H.P., Jr., 1979. Oxygen and hydrogen isotope relationships in hydrothermal mineral deposits. *In Geochemistry of Hydrothermal Ore Deposits* (2nd ed.): New York (Wiley), 236–277.

Vanko, D.A., 1988. Temperature, pressure, and composition of hydrothermal fluids with their bearing on the magnitude of tectonic uplift at mid-ocean ridges, inferred from fluid inclusions in oceanic layer 3 rocks. *J. Geophys. Res.,* 93:4595–4611.

Vanko, D.A., Bodnar, R.J., and Sterner, S.M., 1988. Synthetic fluid inclusions, VIII. Vapour saturated halite solubility in part of the system NaCl-$CaCl_2$-H_2O, with application to fluid inclusions from oceanic hydrothermal systems. *Geochim. Cosmochim. Acta,* 52:2451–2456.

Vanko, D.A., Griffith, J.D., and Erickson, C.L., 1992. Calcium-rich brines and other hydrothermal fluids in fluid inclusions from plutonic rocks, Oceanographer Transform, Mid-Atlantic Ridge. *Geochim. Cosmochim. Acta,* 56:35–47.

Von Damm, K.L., 1990. Seafloor hydrothermal activity: black smoker chemistry and chimneys. *Annu. Rev. Earth Planet. Sci.,* 18:173–204.

Von Damm, K.L., and Bischoff, J.L., 1987. Chemistry of hydrothermal solutions from the southern Juan de Fuca Ridge. *J. Geophys. Res.,* 92:11334–11346.

Von Damm, K.L., Edmond, J.M., Measures, C.I., and Grant, B., 1985. Chemistry of submarine hydrothermal solutions at Guaymas Basin, Gulf of California. *Geochim. Cosmochim. Acta,* 49:2221–2237.

Yanatieva, O.K., 1946. Polythermal solubilities in the system $CaCl_2$-$MgCl_2$-H_2O and $CaCl_2$-NaCl-H_2O. *Zh. Priklad. Khim.,* 19:709–722.

Date of initial receipt: 26 February 1993
Date of acceptance: 23 August 1993
Ms 139SR-233

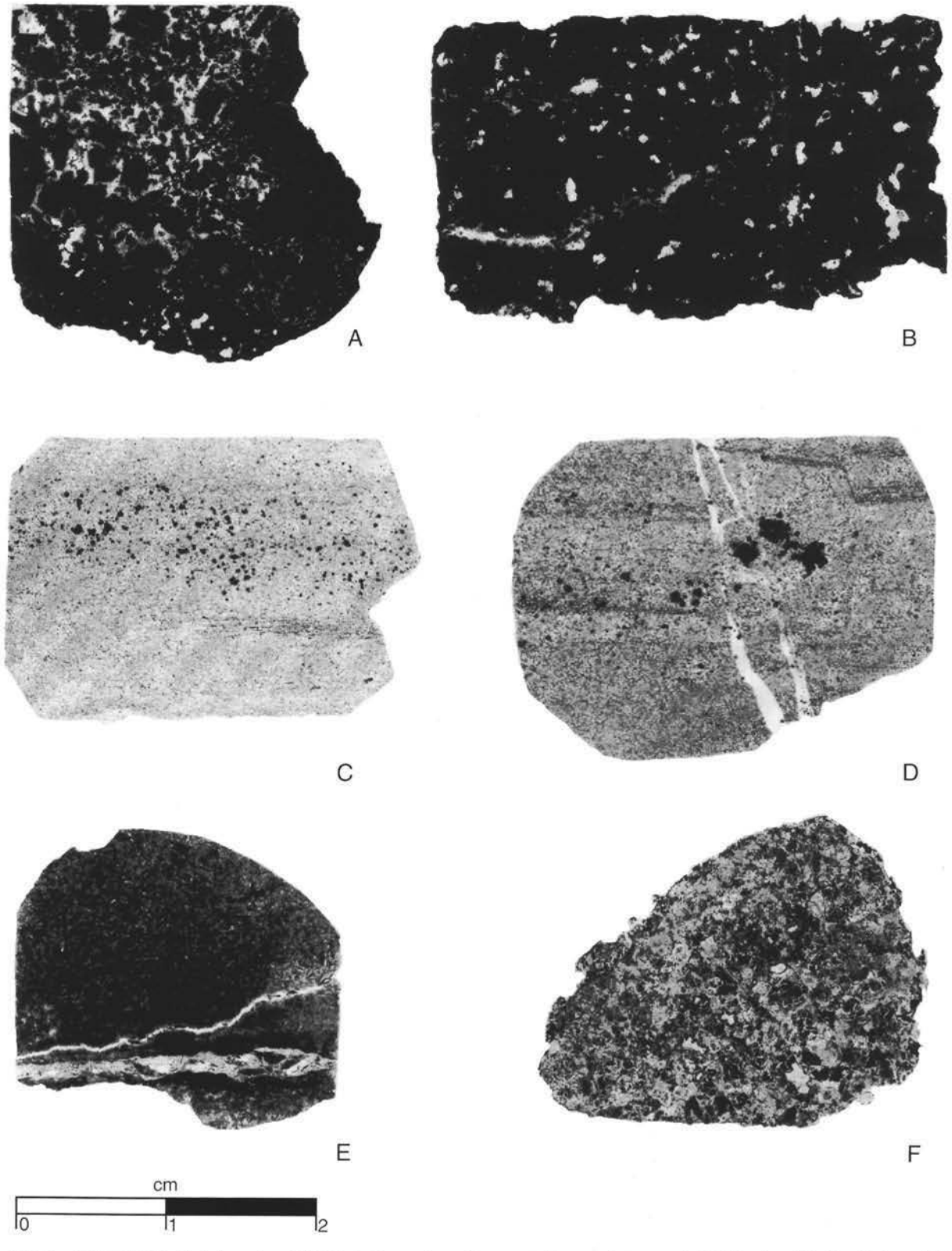

Plate 1. Transmitted light photographs of fluid inclusion sections of representative sample types. **A.** Sulfide clasts (black) with interstitial dolomite matrix (white), Sample 856F-2X-CC, 23–25 cm. **B.** Medium- to coarse-grained sulfide (pyrite-pyrrhotite-magnetite) (black) with interstitial carbonate matrix and cross-cutting calcite veinlet (both white), Sample 856H-3R-2, 135–138 cm. **C.** Indistinctly, thinly laminated fine-grained sediment (white to gray) with fine-grained, disseminated pyrite restricted to a zone, Sample 857D-17R-1, 34–36 cm. **D.** Finely laminated fine-grained sediment (white to gray) with fine-grained disseminated pyrite (black) and cross-cutting wairakite veinlet (white) which offsets bedding, Sample 857D-17R-2, 53–55 cm. **E.** Mafic sill (gray to black) with cross-cutting quartz-wairakite-epidote veinlet (white), Sample 857C-60R-2, 28–30 cm. **F.** Coarse-grained carbonate concretion (white to gray) with interstitial clay-rich sediment (black), Sample 858C-3H-2, 124–126 cm.

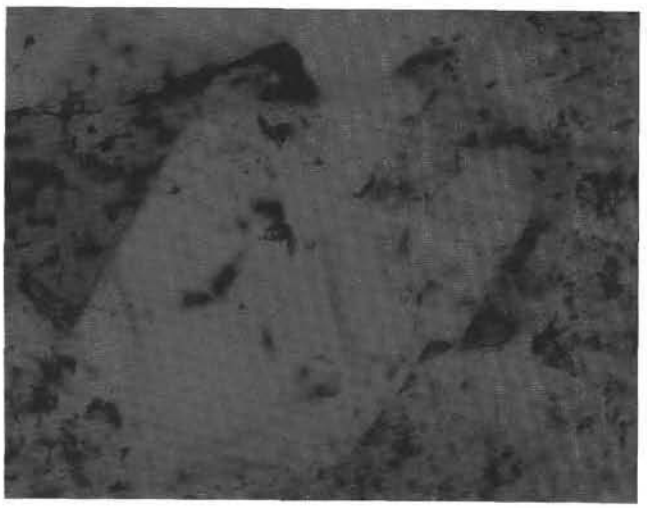

A

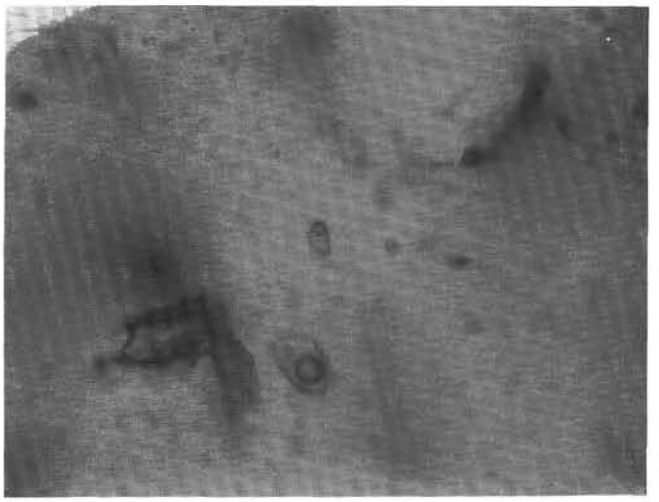

B

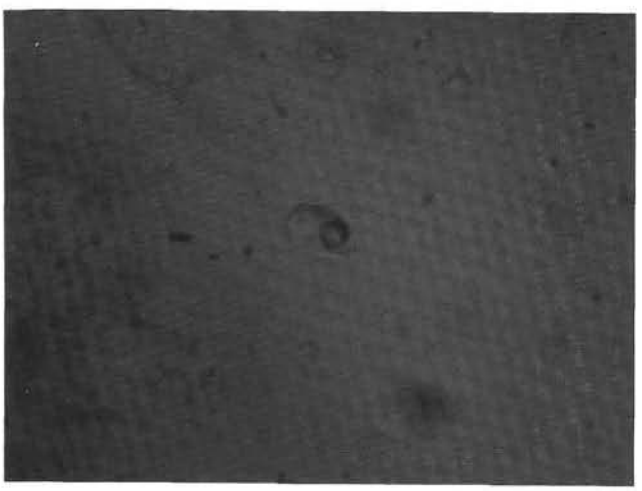

C

D

E

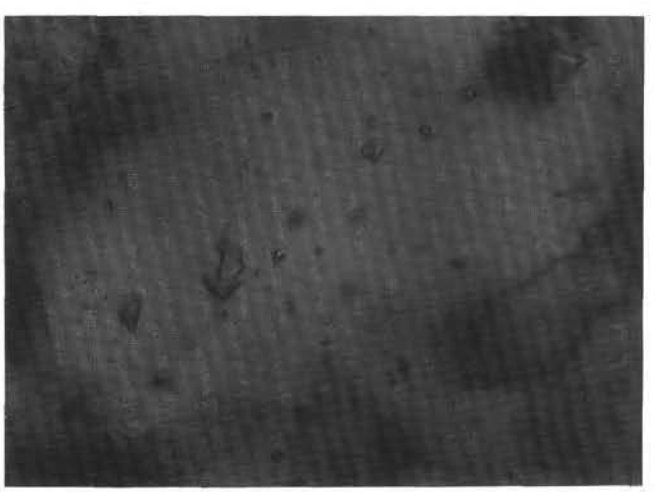

F

Plate 2. Transmitted light photomicrographs of fluid inclusions. **A.** Euhedral quartz crystal with several isolated primary two-phase (L,V) inclusions. Largest inclusion is 30 µm. Sample 858G-16R-1, 77–79 cm. **B.** Close-up of two primary inclusions shown in (A), Sample 858G-16R-1, 77–79 cm. **C.** Primary two-phase (L,V) 35-µm inclusion in quartz, Sample 858A-29X-1, 30–32 cm. **D.** 15-µm-long primary two-phase (L,V) inclusion in low-iron translucent sphalerite in massive sulfide, Sample 856G-7R-4, 4–6 cm. **E.** Planar array of 1- to 5-µm predominantly two-phase (L,V) secondary inclusions along a healed microfracture in anhedral quartz, Sample 857D-17R-1, 34–36 cm. **F.** 2- to 10-µm two-phase (L,V) and one-phase (V) secondary inclusions along several healed microfractures in anhedral quartz, Sample 858A-29X-1, 30–32 cm.

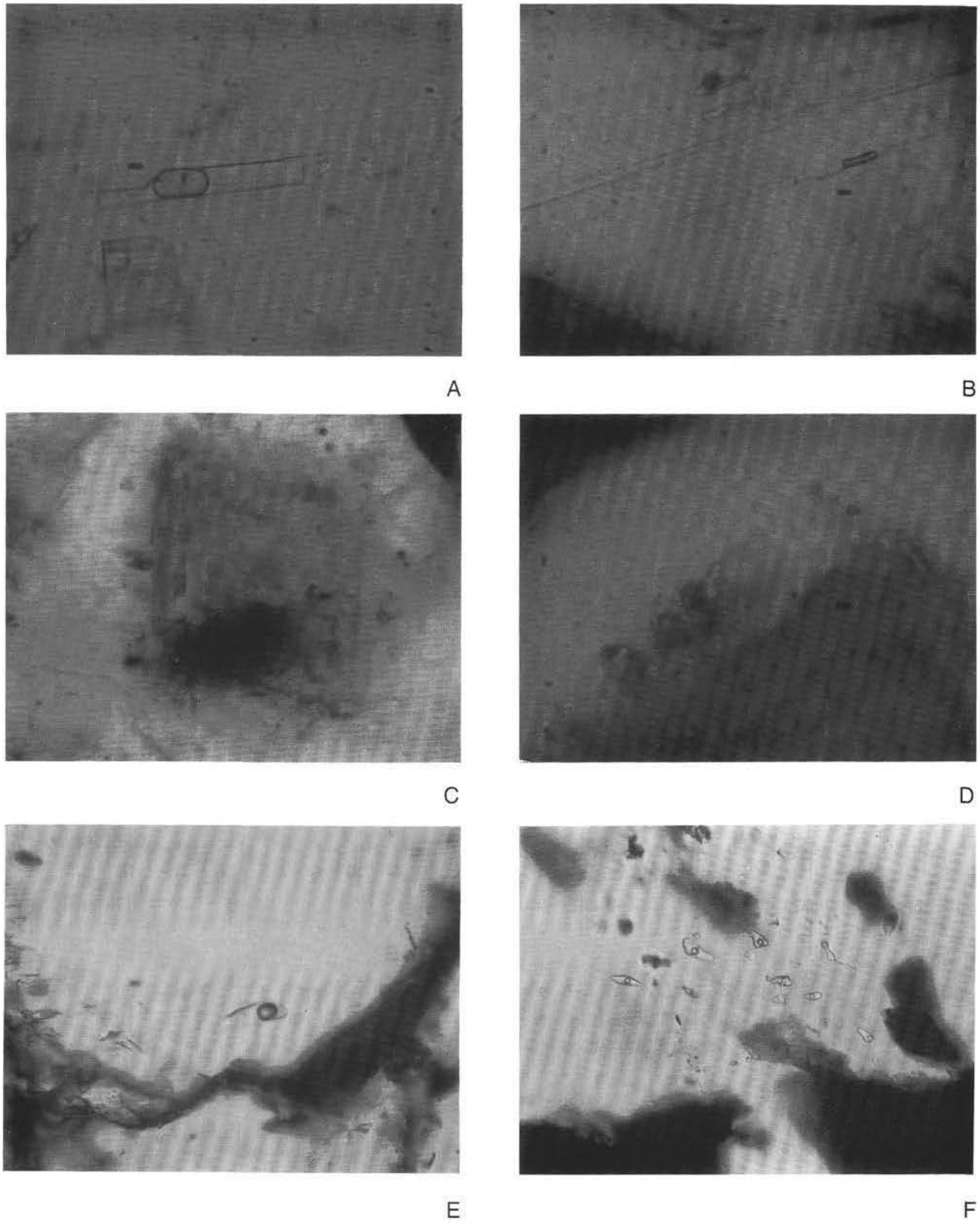

Plate 3. Transmitted light photomicrographs of fluid inclusions. **A.** Rectangular primary two-phase (L,V) 40-µm inclusion in anhydrite, Sample 858A-29X-1, 30–32 cm. **B.** Needle-like primary two-phase (L,V) 70- and 50-µm-long inclusions oriented parallel to cleavage in anhydrite, Sample 857D-1R-1, 137–139 cm. **C.** Growth zones in carbonate defined by primary two-phase (L,V) 2- to 7-µm inclusions and solid inclusions, Sample 856H-3R-1, 28–30 cm. **D.** Close-up of growth zone in carbonate showing irregular 7-µm two-phase (L,V) primary inclusion, Sample 856H-3R-2, 135–138 cm. **E.** Primary two-phase (L,V) 70-µm inclusion in wairakite from quartz-wairakite-epidote vein in mafic sill, Sample 857D-12R-1, 88–90 cm. **F.** Cluster of 10- to 15-µm-diameter secondary two-phase (L,V) inclusions along a fracture in the plane of the fluid inclusion section in quartz from quartz-wairakite vein cutting a mafic sill, Sample 857C-60R-2, 28°30 cm.